Predicting Onset of Damage in Special Class of Laminates under Tension

Nikolaos Kosmas, D.Eng

Supervisor: Dr.ir. Christos Kassapoglou

Delft University of Technology

Predicting Onset of Damage in Special Class of Laminates under Tension

By

Nikolaos Kosmas

In partial fulfilment of the requirements for the degree of

Master of Science
in Aerospace Engineering

at the Delft University of Technology,
to be defended publicly on Wednesday January 7th, 2015 at 14:00

Supervisor:	Prof. dr. ir. Christos Kassapoglou, TU Delft
Thesis committee:	Prof. dr. ir. Derek Gransden, TU Delft
	Christopher Chahine, PhD Candidate, Oxford University, von Karman Institute for Fluid Mechanics, Turbomachinery & Propulsion

This thesis is confidential and cannot be made public until December 31, 2015.

Abstract

In design with composite materials, the capability of tailoring the properties of the structure with respect to the specific load requirements in each direction, allowed by their anisotropic nature, is coupled with the development of interlaminar stresses transferred through the thickness.
Specifically, at the free edge of the laminate, due to the change in fiber orientation and the different response of the constituent materials, stresses that act in the thickness direction are developed. Starting at the free edge and moving towards the center of the laminate up to a certain threshold, the stress state of the plies is further complicated by the interlaminar stresses. The widely employed Classical Laminated Plate Theory does not account for the aforementioned effects, since each ply is considered to be in plane stress state.
The primary goal of the present thesis project was to develop an analytical stress model that includes expressions for all six stresses. By construction, the stresses acting through the thickness have an exponential decay behavior until they become zero, once the aforementioned threshold is reached. Parallel to that, the in-plane stress expressions gradually recover the CLPT predicted values.
Furthermore, the model was intended to capture a specific sequence of damage occurrences in laminates of the family $[0_2/\theta_2/-\theta_2]_s$ loaded under tension, as observed by O'Brien. Namely, during loading matrix cracks initiating at the free edge of the off-axis plies and propagating along the respective fiber orientation are anticipated to occur first. While these cracks increase in length and number, at some point a $+\theta$ crack will intersect with a $-\theta$ one, thus forming an envelope with the free edge. As loading continues, a local delamination is expected within this envelope.
In order to predict that, the stress expressions would have to be implemented in a failure theory that is capable of accounting for the ongoing phenomena and of distinguishing not only between matrix and fiber failure, but also between different matrix failure modes. These requirements led to the selection of Puck Failure Theory.
The process proved to be more complex than estimated and numerous issues occurred during the formulation of the model.
At first, results from literature could not be duplicated. After an extensive period of thoroughly checking and editing the approach, the expressions on a symbolic level and the code in which they were implemented, it was realized that a multiplicative factor is distorting the output.

After calculating the numerical value of the factor for each one of the out-of-plane stress expressions and applying it, agreement with published results was excellent. Unfortunately, the origin of the error could not be found.
Once the error has been corrected, the potential integration of the expressions in a fatigue life evaluation model specifically designed for composites, could replace the currently employed semi-empirical theories that where originally formulated for isotropic materials and rely mainly on curve-fitting.

Acknowledgements

First and foremost, I would like to thank my supervisor, Professor Christos Kassapoglou, for the global experience of conducting a thesis next to him. As a Greek would say, this project was a very important "school" for me, since Christos is not only a brilliant professor and researcher, but also a gifted teacher. During this thesis project together we came across numerous intriguing but also sometimes nerve-racking issues and obstacles but in the end those made the whole process motivating and unique, no matter the outcome.

Furthermore, big thanks to the honorable gentlemen of Room 2.02, Lourens, Nicolas and Jack. Together we made a great team, despite the fact that I had to clean their desks in order to have the tidiest room in the floor (Laura can back me up for that). Besides the fun part, their input in my project helped me go through obstacles when I was frustrated. An extra "credit" to my friend Lourens, for the long yet exciting lab hours we spent together.

Continuing, I would like to mention my housemates Vangelis, Panos, Athinodoros, Kostis, Chris, Kostas, as well as the occasional George from Brussels, that helped and coped with me when I returned home upset at my model. They played a crucial role in making the year of my MS Thesis the best in Delft and not only.

Last but not least, I would like to thank my parents, since without their support I wouldn't have had the chance to have this experience.

Contents

List of Figures

List of Tables

1 General Background

1.1 Introduction

The use of composite materials in primary load bearing structural components has been gaining increasing attention over the last years, especially in industries such as Aerospace, Marine, Automotive and Wind Energy.

In general, when it comes to applications where weight minimization is a crucial factor, composites are superior to traditionally used metals due to their high specific properties. Moreover, their anisotropic nature and performance allows for fine tuning of the structure according to the requirements in each direction, instead of a global behaviour that applies to all planes and directions, which is the case with metals. The level of anisotropy of a composite material system and therefore of a structure or component is also tuneable, based on the selection of materials and the structural design strategy. Hence, it seems that the use of composites is a one way road when the factors discussed above are of interest.

On the other hand, the anisotropic nature of composites is coupled with a variety of damage mechanisms and failure modes, which may act individually, in a unique sequence or even simultaneously. The interactions of the different damage modes and the accumulation of damage starting from initiation up to final failure are crucial in order to have a good understanding of the underlying mechanisms and hence an accurate prediction for design.

1.2 Damage Initiation and Evolution

Whether it is quasi-static or cyclic type of loading, the primary and mostly dominating damage modes in continuous fibre composites are matrix cracking, fibre breakage and delamination. These modes might act singularly or combined, either in an impeding or in a promoting manner with each other.

In the specific load case studied in this project, namely uniaxial tensile quasi-static and potentially cyclic tension-tension loading, the purpose is to isolate matrix cracks in the family of laminates $[0_2/\theta_2/-\theta_2]_s$ and subsequently predict the first matrix cracks and gradually the first delamination.

By formulating a model that can reasonably predict the fatigue performance of the discussed material systems, the design of damage tolerant structures and components is feasible.

Focusing on the matrix of the composite material system, for ductile polymer matrix materials, the fatigue damage evolution resembles up to a certain point that of metals, primarily in the sense that it consists of crack initiation and crack propagation. For Carbon Fibre Reinforced Polymers that are of interest cracks will usually initiate from matrix flaws and propagate until the crack tip reaches a fibre interface, where it will be arrested for some time, until the stress at the crack tip becomes sufficiently high in order to lead to fibre breakage or pass through the thickness to a neighbouring ply. At low strain levels, the formed cracks may be isolated within the matrix itself, increasing only in numbers. This is the so called dispersed matrix failure mode [5].

At higher strain levels, the fibres that are at the crack tip might fail, allowing the matrix cracks to further propagate. If at some point a crack is long enough, the developed shear stress at the crack tip may be high enough to cause interfacial failure, leading to diversion of the crack parallel to the fibre direction. According to the material's interfacial shear strength, the fracture plane might be restrained to a flat surface or a "broom-like" fracture surface [5].

For the family of laminates discussed above, there is a distinct sequence of events that leads from the first damage event to the final catastrophic failure of the laminate. More specifically, matrix cracks are first anticipated in the $\pm\theta$ plies, following the fibre direction in these plies. For the sake of visualization, a crack in the $+\theta$ direction will form an envelope with a crack in the $-\theta$ direction. As cyclic loading continues further on, a delamination is expected to occur within this envelope in the $\theta/-\theta$ interface that will consequently lead to fibre breakage. This is shown schematically in the sketch below.

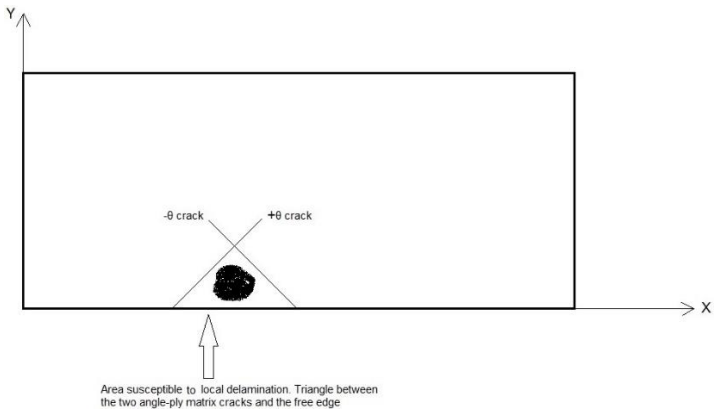

Figure 1: Anticipated damage mode for the $[0_2/\theta_2/-\theta_2]_s$ family of laminates under tension

1.3 State of the Art

Extensive research has been conducted in this field but primarily focusing on cross-ply laminates, consisting of plies in the 0° and the 90° direction. Moreover, glass fibre reinforced polymer (GFRP) material systems are most commonly investigated, since it is possible to visually observe the crack formation within the matrix due to the partial transparency of the samples.

As the density of the cracks in the matrix increases, the appearance of the matrix in that region changes from transparent to more and more opaque/white, indicating the evolution of crack formation.

Extension to other families of laminates was initially studied by O'Brien [6] and O'Brien et al.[7]. In their investigation, cross-ply as well as quasi-isotropic laminates were chosen. The first sequence is chosen in order to isolate and promote the 90° matrix cracking from other damage types. On the other hand, in the second type, the expected damage types are again initially 90° matrix cracks, subsequently followed by free edge delamination in the 0/90 ply interfaces due to the high peeling stresses that are observed at that location. Matrix cracks within a single ply, otherwise named intralaminar cracks, have been observed not to form ad infinitum in number, but only until a certain saturation state is reached, first called by Reifsnider Characteristic Damage State [8]. For the case of cyclic loading, depending on the orientation of each ply, matrix cracks reach their individual saturation level in a different number of cycles [7]. Crack accumulation in the 90° plies is reached prematurely compared to the other ply orientations, so all other damage modes are expected to occur and progress after matrix crack saturation in the aforementioned orientation has been reached.

Whether this concerns quasi-static tension loading or pure tension-tension fatigue loading, the damage sequence and evolution has been observed to be the same. As observed by O'Brien for the stacking sequence $[\pm 30/\pm 30/90/\overline{90}]_s$, the sequence of events is as follows. First of all, a small number of isolated cracks is formed in the 90° plies, followed by small edge delaminations, leading to the formation of more cracks in the 90° plies, along the delaminated length.

Further on, more delaminations occurred up to a point where two of them, initially starting from different sides, joined each other, thus leading to global failure [6].

Dvorak and Laws [9] in their study observed that debonded fibres due to loading are susceptible to be crack initiation locations. Such regions might also be present in the component due to manufacturing flaws etc. Fibre-matrix debonding is more likely to occur in region where the fibre density is increased or if the fibres are in contact.

Another area of particular attention when it comes to cyclic loading is that of stiffness reduction and stress redistribution after the initiation of the crack formation phase described above. For these issues, several shear lag models have been employed [2], [10]. The simplest of the shear lag models is described by Hashin and is based on the assumptions that:

- The normal stress in the applied load direction remains constant throughout the ply thickness
- Shear stresses are only developed in a thin boundary layer of unknown and somehow arbitrary thickness which is located between the plies (interphase)
- The cracks themselves remain sufficiently far apart so that they develop individually and there is no interaction between them.

The main problems associated with the above assumptions are that the transverse normal stresses cannot be estimated, the thickness of the boundary layer is unknown and the fact that the different cracks are not interacting does not agree with experimental findings.

In comparison to the simple shear lag model described above, another method has been proposed by Laws et al [11], who have made used of the Self Consistent Scheme approximation to calculate the stiffness reduction in cracked plies.
Issues associated with this approach include the fact that crack opening restrain due to the neighbouring plies is not taken into account and that stress concentrations due to interlaminar cracks are neglected.
Hashin's variational approach takes into consideration the problems and limitations of the other methods and uses only one assumption, namely that the normal ply stresses in the applied load direction are constant over the ply thickness [2]. The approach is based on the principle of minimum complementary energy.
Berthelot et al. [10], [12]proposed a complete parabolic shear lag model, assuming a linear stress distribution through the ply thickness and consequently a parabolic variation of axial displacement in both 0^{o} and 90^{o} plies.
The different models and approaches that have been suggested are compared to FEM models.
For low crack density values, there is in general a good agreement between the analytical model and the FEM models, but for an increasing crack density some of the models show large discrepancies in their predictions compared to FEM.

Starting from the one-dimensional analytical model, in which the longitudinal stresses are assumed to be constant through the ply thickness, the deviation of the average values between the two methods is considerable.
Continuing with the 2D analytical model, where there is parabolic variation of longitudinal stresses only in the 90° plies, the differences between the model and FEM are reduced. Finally, for the complete parabolic model, that accounts for the longitudinal stress variation in both 0° and 90° layers, a good agreement is achieved compared to the FEM results [10].

1.4 Present Study - Considerations

Considering the various methods presented above, there are some crucial issues that need to be taken into consideration when it comes to damage onset prediction in cross-ply, quasi-isotropic or multi-directional laminates loaded under tension, whether it is quasi-static or cyclic loading. For the case of cross-ply laminates, the interlaminar stresses that are developed due to the large difference in fibre orientation are considerable and should not be neglected.
Furthermore, the same holds for the free edge cracks initiating in the 90° layers. At the location of crack initiation, the out-of-plane stresses are increased, which makes these locations susceptible to delamination.
The issue of edge delaminations was investigated by O'Brien and Hooper [13], who conducted an experimental investigation of the delaminations caused due to the intersection of angle-ply matrix cracks in the off-axis layers of multidirectional laminates of the family $[0_2/\theta_2/-\theta_2]_s$ subjected to static tension.
Through radiography images taken at the onset of damage it was shown that there was at least one and in some cases numerous matrix cracks in the internal $-\theta$ angle plies. For θ values up to 15°-20°, there were only one or two matrix cracks, but, as the θ values increased towards 45°, the number of matrix cracks in the off-axis plies was increased, reaching a maximum of about 10 cracks.
Another interesting observation coming from the radiograph is that there is a triangular dark shadow in some of the specimens (see figure 2, section 1.5). The shadow is enclosed between two matrix cracks, namely in the $+\theta$ and $-\theta$ directions, which are intersecting. The apparent shadow is indicating a local delamination at the intersection between the two matrix cracks at the $+\theta/-\theta$ interface, where the interlaminar stresses are at maximum.

All tests were consistent in the sense that the occurrence of the local delamination was an event following the initial matrix cracking in the $-\theta$ plies. These two events were always coupled in the way that initial matrix cracking in the $-\theta$ was followed by delamination. The normal and shear in-plane stresses, as well as the interlaminar stresses at the edges were calculated using a 3D FEM model. It indicated that matrix cracks are prone to initiate in the $-\theta$ oriented plies that are closest to the mid-plane of the laminate, where the in-plane transverse stresses have the greatest magnitude. Compared to that, the First Ply Failure (FPF) criteria that use the Classical Laminated Plate Theory (CLPT) stresses as an input for damage onset prediction, indicate that failure initiation of a ply is located near the free edge, where the in-plane transverse stresses have their maximum values, but, on the other hand, might be a bit unconservative due to the fact that the stresses calculated from CLPT are actually the ones that are developed in the part of the laminate that is not affected by the interlaminar stress effects. Hence, the predicted stress state might be more "optimistic" than reality.

An important conclusion is that in this class of laminates, free edge delaminations do not expand along the whole length of the laminate, as is observed in other types of laminates, but they exhibit local delaminations near the free edges and these delaminations are always constrained between two matrix cracks, namely in the $+\theta$ and $-\theta$ orientations.

Taking into account all the experimental investigations presented above, it can be realised that it is quite challenging and complex to combine free edge cracking and interlaminar stresses in an analytical model without the use of a finite element analysis.

On the other hand, a FEM simulation of the problem can be prohibitive in a design environment, where long runs might be required in modelling cyclic loading where the model needs to be updated in every cycle to account for strength and stiffness degradation. Hence rises the need for an analytical model that will take into account the interlaminar stresses at the vicinity of the laminates that are affected by the free edge effects. Moreover, the selection of the failure criterion to predict the initiation of ply failure, the first matrix crack, is of critical importance.

1.5 Research Objectives

Taking into consideration all the aforementioned, the primary scope of this thesis project is to:

- Develop an analytical model that will provide the capability to obtain the developed stresses and reliably predict the onset of damage initiation under uniaxial tensile loading for the special class of laminates with stacking sequence $[0_2/\theta_2/\text{-}\theta_2]_s$. The formulation of a three-dimensional stress solution is required, in order to take into account the critical interlaminar stresses that will be developed near the free edges of the laminate.

- This stress solution will gradually lead to the recovery of the classical laminated theory stress state, meaning that on a ply level the out-of-plane stresses will become zero and the in-plane stresses will match the CLPT stress distribution (plane stress). This is expected to take place in the "far-field" portion of the laminate that is not affected by the free edge effects.

- A reliable failure theory will have to be employed, so that it can accurately predict the anticipated damage mode and the point at which it will occur. This should be a criterion that will take into account the stress interactions and that can give an insight on the occurring damage mode and not merely a load or stress state at which first ply failure will occur. Considering the fact that the failure mode that needs to be captured is matrix cracking in specific angles, the failure criterion must make a distinction, not only between fiber and matrix failure, but also between different modes of matrix failure.
- The model should be capable of accounting for the sequence of events and mechanisms leading to failure onset. The sequence of failure events that the model will attempt to capture are, qualitatively, as follows:
    1. The initiation of damage (first ply failure) is expected to be in the form of a matrix crack, occurring in a ply within the block of the off-axis plies located internally in the sequence and at the location of the free edge of the laminate (see figure 2, next page).
    2. The crack will then propagate along the fibre direction, namely either at an angle $+\theta$ or $-\theta$ with respect to the laminate's longitudinal axis.

3. At a certain point during loading, looking at the top view of the laminate (xy plane), a triangle envelope is expected to be formed between the free edge, a $+\theta^{o}$ crack and a $-\theta^{o}$ crack.
4. Continuing, within this envelope, a local delamination is expected to occur.
5. Accumulation of these damage types will subsequently lead to fibre breakage and finally to global failure. Hence, the 3D stress solution will have to be modified in order to account for the first matrix cracks formed in the $\pm\theta$ orientation.

The criterion should have the capability of determining the first matrix cracks and subsequently the triangularly shaped delaminations in the $\theta/\text{-}\theta$ interface.
A characteristic image is shown below, indicating the triangular envelope (dark part – local delamination) that is constrained between two matrix cracks, one in the θ direction and the other one in the $-\theta$.

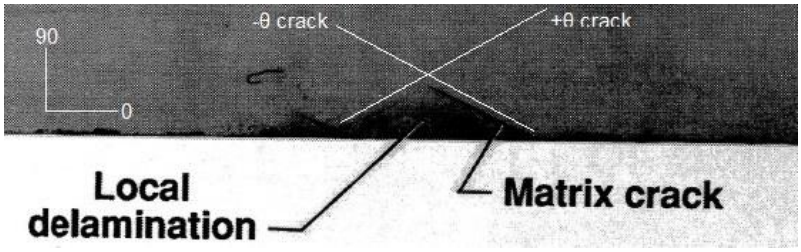

Figure 2: Example of $[0_2/25_2/\text{-}25_2]_s$ laminate after onset of damage [13]

The selection of the $[0_2/\theta_2/\text{-}\theta_2]_s$ family was made because they combine all the major failure modes, namely matrix cracking, delamination and fibre breakage, in a reasonably well-defined sequence.
Thus, a model capturing all events as described above will be very promising for further extension in laminates with other types of stacking sequences.
Finally, extending the considerations to pure tension cyclic loading would allow the possibility of implementing the developed stress solution into a fatigue model based on the cycle-by-cycle probability of failure, stiffness degradation and load redistribution with respect to the predicted damage events.

This could potentially lead to a promising analytical method that does not rely on any semi-empirical methods that are originally applicable to isotropic materials [14], [15].
In what follows, Chapter 2 consists of a review of the most commonly used failure theories for predicting the onset of damage in composite laminated structures. Continuing, it concludes with a more detailed description and analysis of the employed failure theory for the discussed project.
Further on, Chapter 3 is focused on the proposed model that will give the desired three-dimensional stress state. Each step that was taken during the development of the model is mentioned clearly. Moreover, additional information, as well as more details, can be found in the corresponding appendices. The idea is that the reader will get all the required documentation in order to be able to potentially repeat the process.

2 Review of Failure Theories for Composite Materials

As mentioned at the end of the previous chapter, one of the key ingredients of the approach to be developed is the failure criterion that will be used. The present chapter discusses various failure theories and their respective advantages and disadvantages.

2.1 General Discussion

The vast and versatile design opportunities offered by Fiber Reinforced Polymer materials in comparison with their metal competitors and in some cases predecessors and the ability to fine-tune the mechanical properties of the component or structure differently in each direction according to the structural requirements are a consequence of the anisotropic behavior of such materials.

The engineering community has been carrying out longstanding analytical and experimental campaigns in the process of formulating failure theories that can accurately and consistently predict the onset of damage initiation and gradually the evolution of damage in such material systems. The employed assumptions during the design phase, the extent of structural optimization that is to be achieved in each problem and numerous other parameters can either promote or "suppress" the inherent anisotropic characteristics of the discussed material systems. It is widely known that in order to fully exploit the structural capabilities of FRPs, they must not be handled with design strategies that are traditionally applied to metallic materials. This statement is of course coupled with the consequence of increased complexity in predicting the structural performance of composite materials.

During the recent decades, a large number of failure criteria have been developed for composite materials, most of which can be quite simplistic in the assumptions that they include and the stresses that they take into account for the prediction of the onset of damage.

In an attempt to get a better comparison and understanding of the different failure criteria a programme was begun to evaluate failure criteria for fibre composite materials.

This "World Wide Failure Exercise" was conceived and conducted by M. J. Hinton and A. S. Kaddour and others [16], [17].

It functioned for over a decade and involved the participation of many advocates for many different possible approaches to the problem. The results and conclusions of the programme were highly inconsistent even in that case, indicating once more the uncertainty of the failure criteria and the complexity of the phenomena they attempt to quantify.
In the following section, the most commonly employed failure criteria will be briefly reviewed.
At first, the proposed macromechanical models for failure prediction of anisotropic materials were based on the already existing theories for isotropic materials,
including extensions and adaptations that would account for the anisotropy in strength and stiffness of such materials [18].
The common characteristic of most of these theories is the assumption of homogeneity up to some extent, as well as the linear relationship between developed stresses and strains. Another point that must be stressed out is the interaction between the different stress components that most theories fail to take into account and exclude due to their simplifying assumptions. The different theories can be classified in three main categories [19]:

1. Limit Criteria: These criteria predict failure of a structure by comparing the ply stresses in the principal directions with the respective strength in a separate manner. Therefore, no interaction between stresses is considered.

2. Interactive Criteria: According to the given load case, these criteria predict a failure load by using a quadratic or higher order polynomial failure index, that includes all the different stress components. Once the failure index is satisfied, failure has been reached at that corresponding calculated load. This category of failure criteria account for interaction between stresses up to a certain extent, but do not indicate anything with respect to the failure mode.

3. Separate Mode Criteria: The failure theories that fall into this group distinguish between fiber failure and matrix failure. The failure indices can be dependent on either one or more stress components. Hence, the degree of stress interaction that is taken into consideration differs according to the specific theory employed.

Some representative criteria of each of the above mentioned categories will be discussed below [19].

2.2 Limit Criteria

2.2.1 Maximum stress criterion

This criterion is based on the assumption that failure occurs when at least one of the stress components along the principal materials axes exceeds the respective material strength in that direction. The failure condition is:

$$\sigma_1 = \begin{cases} X_T \ when \ \ \sigma_1 \geq 0 \\ X_C \ when \ \ \sigma_1 < 0 \end{cases}$$

$$\sigma_2 = \begin{cases} Y_T \ when \ \ \sigma_2 \geq 0 \\ Y_C \ when \ \ \sigma_2 < 0 \end{cases}$$

$$|\tau_{12}| = S$$

Where X_T and X_C are the tensile and compressive ply strengths in the fiber direction and Y_T, Y_C the ones perpendicular to the fibers. The fiber directions corresponds to subscript 1, while subscript 2 denotes the direction that is perpendicular to the fibers in each ply. It should be mentioned that all the stresses are translated in the local coordinate system of each ply. As it can be seen from the formulation of the criterion, it does not take into consideration any kind of interaction between stresses [19].

2.2.2 Maximum strain criterion

This failure theory is practically the same as the one discussed above, but from a strain point of view instead of stress. Failure occurs when at least one of the strain components in one of the principal material axes exceeds the ultimate strain in that direction. The failure condition is as follows:

$$\varepsilon_1 = \begin{cases} \varepsilon_{1\,T}^{u} \ when \ \ \varepsilon_1 \geq 0 \\ \varepsilon_{1\,C}^{u} \ when \ \ \varepsilon_1 < 0 \end{cases}$$

$$\varepsilon_2 = \begin{cases} \varepsilon_{2\,T}^{u} \; when \;\; \varepsilon_2 \geq 0 \\ \varepsilon_{2\,C}^{u} \; when \;\; \varepsilon_2 < 0 \end{cases}$$

$$\left|\gamma_6\right| = 2 \cdot \left|\varepsilon_{12}\right| = \gamma_6^u$$

Where $\varepsilon_1, \varepsilon_2, \gamma_6$ are the developed strains in the principal material directions. On the right hand side of the failure conditions are the ultimate strains. Subscript "t" indicates tension, "c" indicates compression, "u" means that these are the ultimate strains and the numbers correspond to the respective directions [19].

2.3 Interactive Criteria

2.3.1 Tsai-Hill criterion

In contrast with the previously mentioned criteria, Tsai and Hill were among the first to include a combined failure condition for composite materials. Its principle is directly derived from the von Mises yield criterion, vastly known and used for isotropic materials. The difference lies in the fact that for composite materials instead of yielding there is failure. The Tsai-Hill criterion in its final form is given below [20]:

$$\frac{\sigma_x^2}{X^2} - \frac{\sigma_x \cdot \sigma_y}{X^2} + \frac{\sigma_y^2}{Y^2} + \frac{\tau_{xy}^2}{S^2} = 1$$

Where again X,Y are the corresponding strengths parallel and perpendicular to the fiber direction respectively and S is the in-plane shear strength. Thus, the criterion distinguishes between different strengths in different directions.

2.3.2 Tsai-Wu criterion

This criterion came as an attempt to tweak the previously described Tsai-Hill so that it can account for the fact that composite materials have different strength in tension than in compression. This leads to conclusion that the Tsai-Wu criterion is not merely phenomenological, but is also includes curve fitting. The criterion is [20]:

$$\frac{\sigma_x^2}{X^T \cdot X^C} + \frac{\sigma_y^2}{Y^T \cdot Y^C} - \sqrt{\frac{1}{X^T \cdot X^C} \cdot \frac{1}{Y^T \cdot Y^C}} \cdot \sigma_x \cdot \sigma_y + \left(\frac{1}{X^T} - \frac{1}{X^C} \right) \cdot \sigma_x + \left(\frac{1}{Y^T} - \frac{1}{Y^C} \right) \cdot \sigma_y + \frac{\tau_{xy}^2}{S^2} = 1$$

Superscripts t and c correspond to tension and compression. In both of the above mentioned criteria, the stresses are on a ply-level and with respect to the local coordinate system of the ply and not the global of the laminate.

2.3.3 Hoffman criterion

This criterion has the form:

$$\frac{\sigma_1^2}{X^T \cdot X^C} + \frac{\sigma_2^2}{Y^T \cdot Y^C} + \frac{\tau_{12}^2}{S^2} - \frac{\sigma_1 \cdot \sigma_2}{X^T \cdot X^C} + \left(\frac{1}{X^T} - \frac{1}{X^C} \right) \cdot \sigma_1 + \left(\frac{1}{Y^T} - \frac{1}{Y^C} \right) \cdot \sigma_2 = 1$$

Equivalent to the previously described Tsai-Wu criterion [20], [21]. It basically is a modification of the criterion originally proposed by Hill. The difference lies in the inclusion of linear terms with respect to stress, thus taking into account the different performance of such material systems in tension and compression.

2.4 Separate Mode Criteria

As discussed above, the criteria that fall into that category are the ones that do not solely indicate failure, but also make a distinction between different failure modes.

2.4.1 Hashin-Rotem criterion

It is made up of two separate failure conditions, one indicating fiber failure and another one for matrix failure.

The one of the two that is satisfied first (at a lower stress state) is the one that is considered as the first damage mode that will occur while loading. The two conditions are given below [19]:

$$\frac{\sigma_1}{X} = 1 \ (fiber\,failure)$$

$$\left(\frac{\sigma_2}{Y}\right)^2 + \left(\frac{\tau_{12}}{S}\right)^2 = 1 \ (matrix\,failure)$$

2.4.2 Hashin criterion

The main difference and advantage of that criterion in comparison to the previous one is that instead of just fiber failure, it also gives the capability of predicting whether the fiber failure is in tension or in compression [19]. As it will be seen, the condition for matrix failure is the same as above.

$$\left(\frac{\sigma_1}{X^T}\right)^2 + \left(\frac{\tau_{12}}{S}\right)^2 = 1 \ (fiber\,failure - tension)$$

$$\frac{\sigma_1}{X^C} = 1 \ (fiber\,failure - compression)$$

$$\left(\frac{\sigma_2}{Y}\right)^2 + \left(\frac{\tau_{12}}{S}\right)^2 = 1 \ (matrix\,failure)$$

Due to the fact that now there separate tensile and compressive fiber failure modes, it is necessary to distinguish between X^T and X^C, the first indicating the ply strength in tension and the second one in compression.

2.5 Puck Failure Theory

It can be seen from the brief discussion in the previous section that most failure criteria rely on simplifications, curve fitting, or emulation of metal behaviour. As such, they are not expected to be very accurate, as was demonstrated by the World Wide Failure Exercise [16], [17]. It is very important that the failure criterion or criteria used capture some of the physical mechanisms taking place during failure and at a length scale that allows relating local failure mechanisms with global behaviour.

The need, therefore, arises for a physically based phenomenological model that will not rely on linear stress-strain relationships, will account for various failure modes and at the same time will be practical to use in engineering practice.
For the purposes of the thesis project, the primary criterion that has been selected, which seems to meet these requirements, is the Puck Failure Criterion, which is also the most widely accepted in the Aerospace Industry and was initially formulated for damage onset and fracture [1], [3], [4], [22], [23].

The main reasons for that selection are:

1. It avoids deficiencies of both interactive and non-interactive failure theories
2. It distinguishes between fibre and matrix failure modes, including 3 matrix failure modes and 2 fibre failure modes
3. It relies on non-linear stress and strain analysis before the initiation of failure
4. It includes a physically based action plane related fracture criteria, both for inter-fibre failure and for fibre failure

In contradiction to the analysis of stresses and strains, strength analysis of composite laminates demands the formulation of fracture models that are sufficiently close to physical reality and yet remain practical and feasible for engineering practice. Puck's fracture theory has some distinct characteristics that are judged to be fundamental when the issue of a reliable fracture criterion arises.
These characteristics are:

- Two independent fracture criteria are applied at the same time. One for fiber failure (FF) and one for inter-fiber failure (IFF). This is essential since these two fracture occurrences must be treated as independent phenomena. Moreover, the design strategy is different according to the governing failure mode, the one that will occur at a lower load.
- The fracture envelope of (σ_2, τ_{12}), where 2 is the direction perpendicular to the fibers, is not described by a single equation that included both the transverse tensile strength Y_t and the transverse compressive strength Y_c. The reason for that is that the strength characteristics in tension and compression are independent.
- In the case of IFF type of failure, it is crucial that the criterion gives information whether IFF occurred from transverse tension or compression. The case of crack formation due to transverse tensile stresses is relatively benign, compared to the

respective case in compression, which potentially causes the "explosive" effect of oblique cracks.

Following this introductory part, the fracture theory will now be described in more detail. The failure model is based on the brittle behaviour of composites and it accounts for five different failure modes in total, namely fibre failure in tension and in compression and three different inter-fibre failure modes, namely A, B and C (see Figure 2). Modes A and B concern cracks that develop perpendicular to the mid-plane in tension and compression respectively (straight cracks), while mode C predicts oblique cracks that are at an angle. For mode C, the direction of the crack is also predicted, by means of the inclination of the fracture plane with respect to the thickness direction of the laminate.

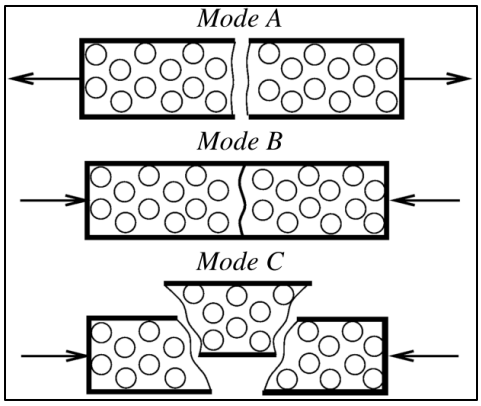

Figure 3: Inter-fiber failure modes of Puck failure theory [1]

According to Puck's criterion, there are six types of stresses (Figure 4) that can cause fracture, namely tension and compression parallel to the fibre direction (associated with the two fibre failure modes), then tension and compression perpendicular to the fibre direction and two types of shear stress, perpendicular-perpendicular,
shearing the 13 or the 12 planes (3being the out-of-plane direction) and parallel-perpendicular, shearing the 23 plane (associated with the three inter-fibre failure modes). Instead of the common stress subscript notation, Puck introduced the term of "stressing" only distinguishing whether the stress is acting longitudinally or transversely to the fibre direction. The stressings are shown below in Figure 4 for better understanding.

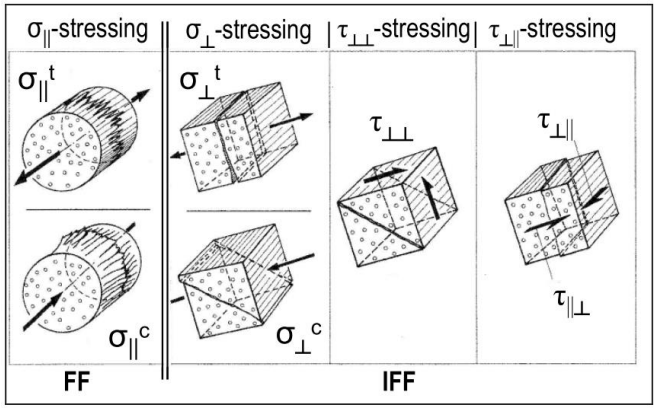

Figure 4: The six types of stressing of Puck failure theory [2]

Corresponding to the six "stressings" mentioned above, there are also six strengths that are taken into account by the criterion, which are the experimentally determined ultimate loads for each type of stressing divided by the surface on which the load is acting. A point of attention related to the surface on which the stress is acting is that in the case of brittle fracture, as it is in CFRP and GFRP with brittle epoxy matrix, is that it does not coincide with the fracture plane.

The only stressings that produce fracture in their action planes with the action plane coinciding with the fracture plane are tensile perpendicular to the fibre direction and perpendicular-parallel shear, shearing the 23 plane.

Therefore, it can be concluded that we are dealing primarily with brittle fracture behaviour and that criteria which are originally intended for ductile metallic materials are not applicable.

Therefore, the essential fracture hypothesis that needs to be followed in our case is that "The stresses in the fracture plane are decisive for fracture", as formulated initially by Mohr. This idea was adopted by Puck in the formulation of his fracture criterion and tuned in order to apply to UD composites. The resulting hypothesis is that the normal stress σ_n and the shear stresses τ_{nt} and τ_{n1} are critical for inter-fibre failure.

A tensile stress promotes fracture whereas a compressive stress impedes fracture, acting as a crack closure mechanism. See Figure 4 below for reference.

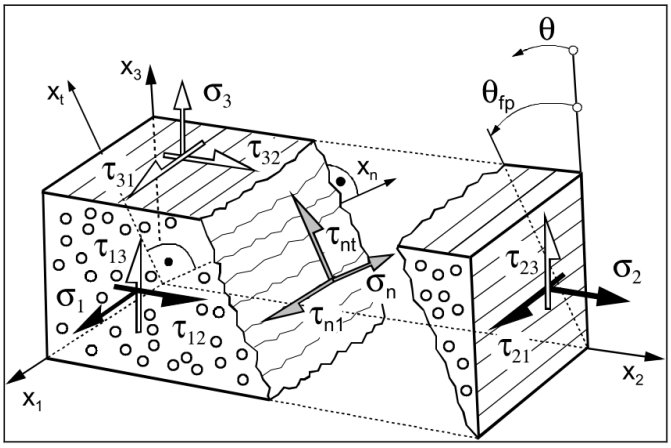

Figure 5: Acting stresses on the fracture plane [3]

Another term that is introduced by Puck in his criterion is that of the fracture resistance R^A (superscript stands for action plane).

The fracture resistance of an action plane is the maximum resistance with which the action plane can resist its own fracture caused either by tensile stressing perpendicular to the fibre direction, a transverse-transverse (namely 12 or 13) shear or a transverse-parallel (23) shear stressing.

Finally, another term incorporated in Puck's failure theory is that of the master fracture body. It concerns the inter-fibre failure modes and envelopes all the possible stress states that the unidirectional composite can withstand without damage/fracture.

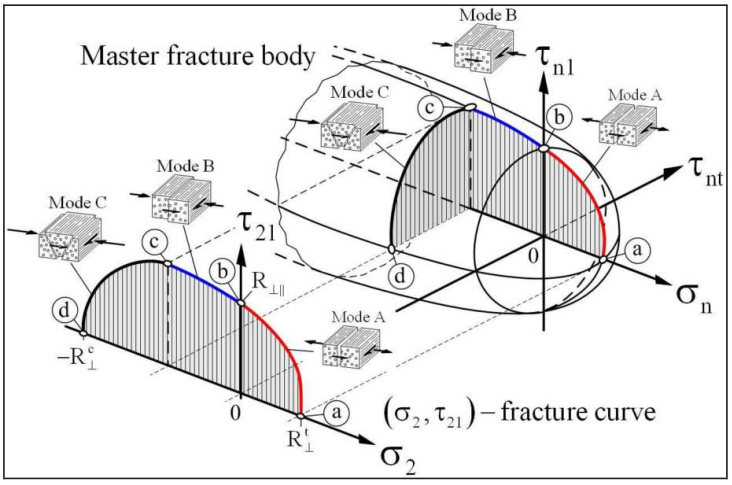

Figure 6: Puck's master fracture body [3]

A point of attention is the determination of the fracture plane angle θ_{fp} (see Figure 5) that concerns mode C IFF (inter-fibre failure).

It is essential to know the fracture plane angle in order to be able to determine the direction of the fracture vector that will give mode C failure.
The answer follows from the fact that fracture is expected at the plane that is parallel to the fibre direction and that the stress state under consideration has its maximum value.
The failure indices for Puck's failure theory for each failure mode are given below.

Failure Mode	Failure Index
Fibre Tension	$\frac{E_L}{X^T} * \left(\varepsilon_L + \frac{v_f}{E_f} * m_{\sigma f} * \sigma_T\right) = FI_f, \qquad (\ldots) \geq 0$
Fibre Compression	$\frac{E_L}{X^C} * \left\|\left(\varepsilon_L + \frac{v_f}{E_f} * m_{\sigma f} * \sigma_T\right)\right\| = FI_f, \qquad (\ldots) < 0$
Mode A	$\sqrt{\frac{\tau_{TL}^2}{S} + \left(1 - p_{\perp\parallel}^{(+)} * \frac{Y^T}{S}\right)^2 * \left(\frac{\sigma_T}{Y^T}\right)^2} + p_{\perp\parallel}^{(+)} * \frac{\sigma_T}{S^T} = FI_M, \qquad \sigma_T \geq 0$
Mode B	$\frac{1}{S} * \left(\sqrt{\tau_{TL}^2 + \left(p_{\perp\parallel}^{(-)} * \sigma_T\right)^2} + p_{\perp\parallel}^{(-)} * \sigma_T\right) = FI_M, \quad \sigma_T < 0 \leq \left\|\frac{\sigma_T}{\tau_{TL}}\right\| \leq \frac{R}{\|S_c\|}$
Mode C	$\left[\left(\frac{\tau_{TL}}{Y^C} * \frac{R}{S}\right)^2 + \left(\frac{\sigma_T}{Y^C}\right)^2\right] * \frac{Y^C}{-\sigma_T} = FI_M, \quad \sigma_T < 0 \leq \left\|\frac{\tau_{TL}}{\sigma_T}\right\| \leq \frac{\|S_c\|}{R}$
	$R = \frac{Y^C}{2 * \left(1 + p_{\perp\perp}^{(-)}\right)}, \quad p_{\perp\parallel}^{(+)} = p_{\perp\parallel}^{(-)} = p_{\perp\perp}^{(-)} * \frac{S}{R}, \quad S_C = S * \sqrt{1 + 2 * p_{\perp\perp}^{(-)}}$

Table 1: Puck's failure indices

The following table is explanatory of the required parameters and properties for the application of the criterion.

X^T, X^C	Longitudinal tensile and compressive ply strength
Y^T, Y^C	Transverse tensile and compressive ply strength
S	In-plane shear ply strength
E_f, v_f	Fiber modulus and Poisson's ratio
$p^{(+)}{}_{\perp\perp}$, $p^{(-)}{}_{\perp\perp}$, $p^{(+)}{}_{\parallel\perp}$, $p^{(-)}{}_{\parallel\perp}$	Inclination parameters that are experimentally determined
$m_{\sigma f}$	Stress magnification factor due to difference between fiber transverse modulus and matrix modulus
E_L	Ply longitudinal Young's modulus

ε_L	Normal longitudinal strain
σ_T, τ_{TL}	Transverse normal and in-plane shear ply stress

Table 2: Required parameters for the application of Puck failure criterion [4]

For the case of IFF mode C, the fracture plane angle with respect to the thickness direction (see Figure 5) is given by the formula [22]:

$$\theta_{fp} = \arccos\sqrt{\frac{1}{2\left(1+p_{\perp\perp}^{(-)}\right)}\left[\left(\frac{\tau_{21}}{\sigma_2}\right)^2\left(\frac{R_{\perp\perp}^{A}}{S_{21}}\right)^2+1\right]}$$

Typical values are also given below for the inclination parameters [23].

	$P_{\perp\perp}^{(-)}$ [−]	$p_{\perp\perp}^{(+)}$[−]
GRP	0.20 to 0.25	0.20 to 0.25
CFRP	0.25 to 0.30	0.25 to 0.30

Table 3: Recommended values for inclination parameters

The model described above was applied to numerous cases of different laminates (both GFRP and CFRP) and under different loading schemes. Typical results of the anticipated fracture envelopes will be described below.

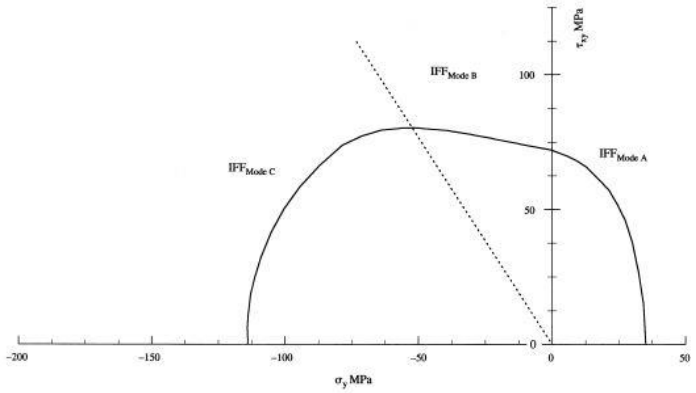

Figure 7: Biaxial failure stress envelope of GRP laminate [4]

In the figure above, the failure envelope is shown for GFRP material under combined transverse and shear loading.

Three different failure modes are included in the envelope, depending on the developed stress state. Namely, under combined in-plane shear and transverse tension, IFF mode A occurs.

At low levels of transverse compression (combined always with shear), IFF mode B occurs. At stress combinations that are on the left of the dashed line (that indicates higher levels of transverse compression), IFF mode C is the predicted failure mode.

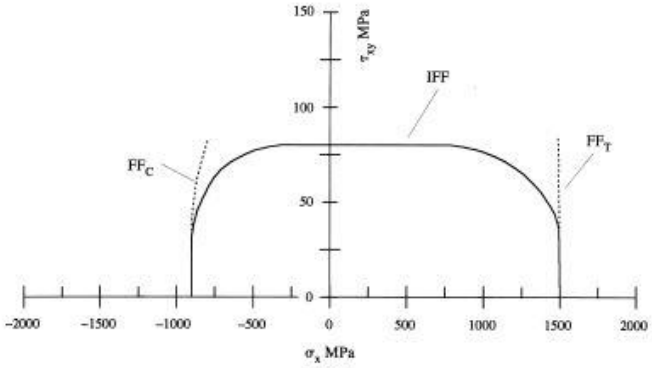

Figure 8: Biaxial failure envelope of CRP laminate [4]

Figure 8 displays the failure envelope of a CFRP laminate subjected to longitudinal loading combined with in-plane shear. The different load regions and combinations again indicate a different mode of failure.

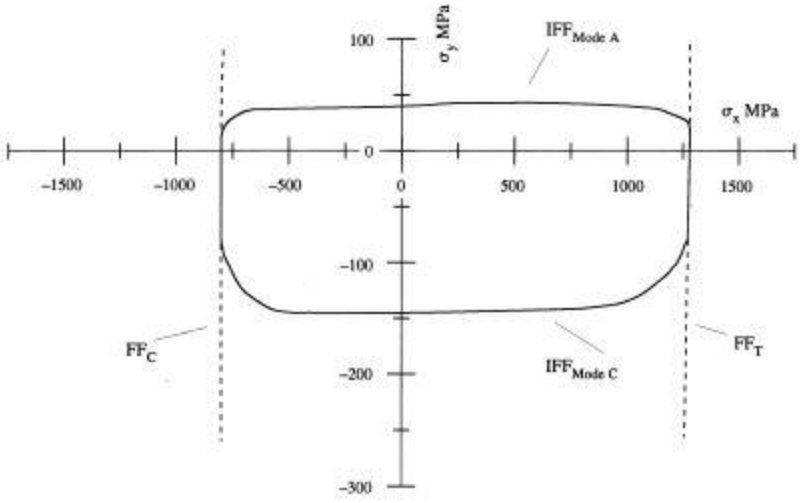

Figure 9: Biaxial failure envelope of GRP laminate [4]

A GRP laminate under combined longitudinal and transverse axial stress is shown in Figure 9. In this case, four different failure modes are observed.
There is both fiber failure in tension and compression and naturally it is observed on the vertical boundaries of the envelope, where the longitudinal axial stress has its maximum absolute values.

In between those two limits, the occurring failure modes are either IFF mode A or mode C, depending on the sign of the transverse stress.
As it can be observed from what was mentioned above, the matrix failure modes that are experimentally observed such as cracks that have propagated either perpendicular or inclined with respect to the fiber plane (12), are captured by the Puck failure theory.
It gives a better insight on the type of failure that should be anticipated, depending on the load (or stress in that case) combination, thus allowing for structural optimization to be oriented specifically with respect to the failure mode that will occur at lower loading regimes. It is a very useful tool to get an overview of the different responses that should be expected in each case. Hence, it is the selected failure theory to be applied in this project. As a reference, the results given in each case by Puck will be compared to the results given by a limit criterion, namely the maximum stress criterion and also to the results by an interactive criterion which, in this case, is the Hoffman failure criterion.

3 Developed Model

3.1 Introductory Discussion

In this chapter, the proposed approach for the determination of the onset of damage in a specific class of laminates under tension will be presented in detail.

More specifically, the examined family of laminates, with stacking sequence $[0_2/\theta_2/\text{-}\theta_2]_s$, is expected to exhibit a certain sequence of damage events when being exposed to this specific type of loading. The phenomenon that is desired to be captured is first of all the matrix cracks propagating along the $\pm\theta$ fiber orientation, followed by a local delamination in the envelope formed between a $+\theta$ crack, a $-\theta$ crack and a free edge of the laminate [6].

It can be understood that it is essential for the model to include in the analysis the out-of-plane stresses, thus taking into account the developed interlaminar stresses and their effects in the vicinity of the laminate that is affected by the free edges.

Further on, as it was briefly mentioned in the first chapter, the functional form for the stresses of the model must at some point lead to the recovery of the Classical Laminated Plate Theory (CLPT) stress solution. As one moves from the free edges towards the center of the laminate, the effects of the interlaminar stresses diminish and, at some point, cease to exist or in any case become negligible. From that point onwards, the predicted stress values of the model should match the ones supplied by CLPT.

Therefore, the stress functions must consist of two parts, one of them accounting for the interlaminar stresses that will become zero after the threshold of the influence of the free edge effects is reached and another one that will handle the part where the stress functions must give the CLPT solutions [24].

All the necessary steps for the formulation of the described model will be shown in the coming sections.

3.2 Initial Stress Expressions

The selected stress functions to be given as a starting point for the derivation of the rest of them are the ones of σ_y and τ_{xy}.

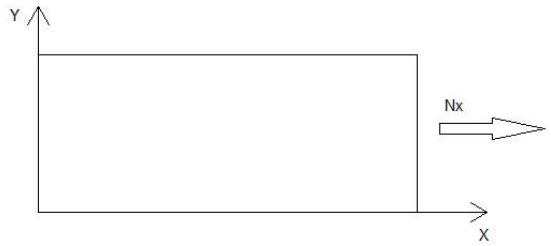

Figure 10: Coordinate system and type of loading

Figure 10 indicates the used coordinate system (global) and the considered type of loading. It should be mentioned at this point that for all the stress functions, no dependence on x is taken into account. All of them have a dependence on the y axis (in-plane dependence) and on the thickness direction (z axis). As it will be realized later on in the description of the model, this assumption was made in order to decrease the number of unknown constants and coefficients to a level that can be handled by the available equations and conditions and to make the model more practical from a mathematical and computational point of view without sacrificing its accuracy and applicability.
Therefore, the initial stress functions are the following:

$$\sigma_y(y,z) = \left(1 + B_1 e^{-\frac{\phi_1 y}{h}} + B_2 e^{-\frac{\phi_2 y}{h}}\right)\left(\sum_{m=1}^{\infty} D_m \cos\left(\frac{2m\pi z}{h}\right)\right) \qquad (1)$$

$$\tau_{xy}(y,z) = \left(1 + A_1 e^{-\frac{\phi_1 y}{h}} + A_2 e^{-\frac{\phi_2 y}{h}} + A_3 e^{-\frac{\phi_3 y}{h}}\right)\left(\sum_{m=1}^{\infty} C_m \cos\left(\frac{2m\pi z}{h}\right)\right) \qquad (2)$$

From the form of the functions given above, it can be seen that they consist of an exponential part with respect to the y direction, multiplied by an infinite Fourier series with respect to z. The origin of the y axis is at the edge, with a direction towards the center of the laminate, see Figure 11 [25].

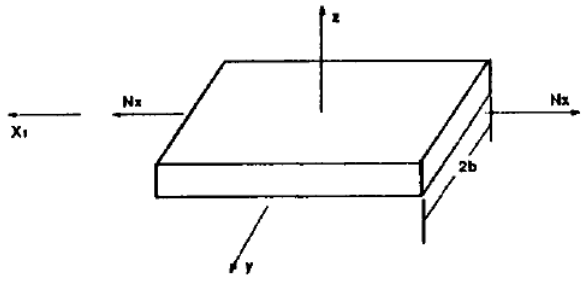

Figure 11: Coordinate system origin

Further on, the unknown constants $\varphi_1, \varphi_2, \varphi_3$ are considered to be positive real numbers. This has as a consequence that when y goes to infinity, all the exponents go to zero, thus leaving only the Fourier series part active. In this case, infinity is considered to be the far-field area of the laminate, where there is no effect of the interlaminar stresses.
Therefore, it remains for the Fourier series to "simulate" the response of the laminate in a way that will match the CLPT stress solution.
The next step is to derive the rest of the stress expressions, through the application of the governing equations for the three-dimensional state of stress. The set of equations is given below.

$$\frac{\partial}{\partial x}\sigma_x + \frac{\partial}{\partial y}\tau_{xy} + \frac{\partial}{\partial z}\tau_{xz} = 0 \qquad (3)$$

$$\frac{\partial}{\partial x}\tau_{xy} + \frac{\partial}{\partial y}\sigma_y + \frac{\partial}{\partial z}\tau_{yz} = 0 \qquad (4)$$

$$\frac{\partial}{\partial x}\tau_{xz} + \frac{\partial}{\partial y}\tau_{yz} + \frac{\partial}{\partial z}\sigma_z = 0 \qquad (5)$$

The red parts of the equations shown above are not existing in the described case since, as already mentioned, no dependence of the stresses on x is taken into account. However, through the elimination of the red terms, it can be seen that in order to solve for σ_x an extra equation is required. By performing a double z integration, it is possible to have an expression for σ_x using the following equation:

$$S_{11}\cdot\frac{\partial}{\partial z}\frac{\partial}{\partial z}\sigma_x + S_{12}\cdot\frac{\partial}{\partial z}\frac{\partial}{\partial z}\sigma_y + S_{13}\cdot\frac{\partial}{\partial z}\frac{\partial}{\partial z}\sigma_z = 0 \qquad (6)$$

This process will be adequately explained in steps in the following sections of the chapter.

3.3 Derivation of the Remaining Stress Expressions

3.3.1 Application of the governing equations - equilibrium

By applying the equilibrium conditions given above, the desired stress expressions are firstly described as shown below:

$$\tau_{xz}(y,z) = -\left(\int \frac{\partial}{\partial y}\tau_{xy}(y,z)\,dz\right) \qquad (7)$$

$$\tau_{yz}(y,z) = -\left(\int \frac{\partial}{\partial y}\,\sigma_y(y,z)\,dz\right) \quad (8)$$

$$\sigma_z(y,z) = -\left(\int \frac{\partial}{\partial y}\,\tau_{yz}(y,z)\,dz\right) + f(y) \quad (9)$$

$$\sigma_x(y,z) = -\frac{\iint\left(S_{12}\left(\frac{\partial}{\partial z}\left(\frac{\partial}{\partial z}\,\sigma_y(y,z)\right)\right) + S_{13}\left(\frac{\partial}{\partial z}\left(\frac{\partial}{\partial z}\,\sigma_z(y,z)\right)\right)\right) dz\,dz}{S_{11}} + K_{star} \quad (10)$$

3.3.2 Application of the boundary conditions

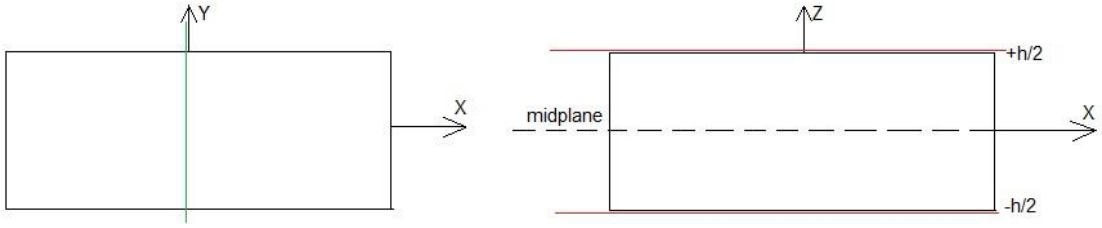

Figure 12: Schematic representation of the applied boundary conditions

The next step is to apply the free edge boundary condition (see Figure 12). This condition ensures that at the origin of the y axis (green line in left part of Figure 12), all stresses that are exposed there (σ_y, τ_{xy}, τ_{yz}) are equal to zero. The condition is given below:

$$\sigma_y(y,z)\Big|_{y=0} = 0 \quad (11)$$

$$\tau_{xy}(y,z)\Big|_{y=0} = 0 \quad (12)$$

$$\tau_{yz}(y,z)\Big|_{y=0} = 0 \quad (13)$$

Applying the above condition to the stress expressions derived previously leads to:

$$(1 + B_1 + B_2)\left(\sum_{m=1}^{n} D_m \cos\left(\frac{2\,m\,\pi\,z}{h}\right)\right) = 0 \quad (14)$$

$$\left(1 + A_1 + A_2 + A_3\right)\left(\sum_{m=1}^{n} C_m \cos\left(\frac{2\,m\,\pi\,z}{h}\right)\right) = 0 \quad (15)$$

$$-\frac{1}{2}\,\frac{\left(-\frac{B_1\,\phi_1}{h} - \frac{B_2\,\phi_2}{h}\right)\left(\sum_{m=1}^{n} \frac{D_m\,h\sin\left(\frac{2\,m\,\pi\,z}{h}\right)}{m}\right)}{\pi} = 0 \quad (16)$$

By solving the system of the three parts included in the parentheses, it is possible to express B_1, B_2 and A_3 with respect to the rest of the unknowns. Further on, the next objective is that the boundary condition at the top and bottom of the laminate is satisfied. This requires that all the stresses that include a z component, meaning τ_{xz}, τ_{yz}, σ_z, must be zero at the outermost boundary of each half of the laminate (red lines in right part of Figure 12).

Since, the mid-plane is considered to be the origin of the coordinate system, this holds for $z=\pm\ h/2$, where h is the total laminate thickness (see Figure 12). The condition is the following:

$$\tau_{xz}(y,z)\Big|_{z=\pm\frac{h}{2}} = 0 \quad (17)$$

$$\tau_{yz}(y,z)\Big|_{z=\pm\frac{h}{2}} = 0 \quad (18)$$

$$\sigma_z(y,z)\Big|_{z=\pm\frac{h}{2}} = 0 \quad (19)$$

From this we get to:

$$\frac{1}{2}\,\frac{1}{\pi}\left(\left(-\frac{A_1\,\phi_1\,e^{-\frac{\phi_1\,y}{h}}}{h} - \frac{A_2\,\phi_2\,e^{-\frac{\phi_2\,y}{h}}}{h} - \frac{\left(-1 - A_1 - A_2\right)\phi_3\,e^{-\frac{\phi_3\,y}{h}}}{h}\right)\left(\sum_{m=1}^{n} \frac{C_m\,h\sin(m\,\pi)}{m}\right)\right) = 0 \quad (20)$$

$$\frac{1}{2}\frac{\left(-\frac{\phi_2\phi_1 e^{-\frac{\phi_1 y}{h}}}{(\phi_1-\phi_2)h}-\frac{\phi_2\phi_1 e^{-\frac{\phi_2 y}{h}}}{(\phi_2-\phi_1)h}\right)\left(\sum_{m=1}^{n}\frac{D_m h\sin(m\pi)}{m}\right)}{\pi}=0 \qquad (21)$$

$$-\frac{1}{4}\frac{\left(\frac{\phi_2\phi_1^2 e^{-\frac{\phi_1 y}{h}}}{(\phi_1-\phi_2)h^2}+\frac{\phi_1\phi_2^2 e^{-\frac{\phi_2 y}{h}}}{(\phi_2-\phi_1)h^2}\right)\left(\sum_{m=1}^{n}\frac{D_m h^2\cos(m\pi)}{m^2}\right)}{\pi^2}+f(y)=0 \qquad (22)$$

For clarification, it should be mentioned that for the interlaminar stresses under discussion (τ_{xz}, τ_{yz} and σ_z), the equations were equivalent for the top and the bottom ply condition, thus giving one condition for each one of the three stresses (with the respective order in which they were mentioned above).

As it can be observed, the first two equations are by default satisfied for all the values of m=1, 2…n, obviously due to the sinus. And from the third one, the unknown function f(y) can be expressed with respect to the rest of the unknown parameters as follows.

3.3.3 Stress functions after equilibrium and BC's

After all the steps described above, the stress functions in their latest form are:

$$\sigma_x(y,z)=-\frac{1}{S_{11}}\left(S_{12}\left(1+\frac{\phi_2 e^{-\frac{\phi_1 y}{h}}}{\phi_1-\phi_2}+\frac{\phi_1 e^{-\frac{\phi_2 y}{h}}}{\phi_2-\phi_1}\right)\left(\sum_{m=1}^{n}D_m\cos\left(\frac{2m\pi z}{h}\right)\right)\right.$$
$$\left.-\frac{1}{4}\frac{S_{13}\left(\frac{\phi_2\phi_1^2 e^{-\frac{\phi_1 y}{h}}}{(\phi_1-\phi_2)h^2}+\frac{\phi_1\phi_2^2 e^{-\frac{\phi_2 y}{h}}}{(\phi_2-\phi_1)h^2}\right)h^2\left(\sum_{m=1}^{n}\frac{D_m\cos\left(\frac{2m\pi z}{h}\right)}{m^2}\right)}{\pi^2}\right)+K_{star}$$

$$\sigma_y(y,z)=\left(1+\frac{\phi_2 e^{-\frac{\phi_1 y}{h}}}{\phi_1-\phi_2}+\frac{\phi_1 e^{-\frac{\phi_2 y}{h}}}{\phi_2-\phi_1}\right)\left(\sum_{m=1}^{n}D_m\cos\left(\frac{2m\pi z}{h}\right)\right)$$

$$\tau_{xy}(y,z)=\left(1+A_1 e^{-\frac{\phi_1 y}{h}}+A_2 e^{-\frac{\phi_2 y}{h}}+(-1-A_1-A_2)e^{-\frac{\phi_3 y}{h}}\right)\left(\sum_{m=1}^{n}C_m\cos\left(\frac{2m\pi z}{h}\right)\right)$$

$$\tau_{xz}(y,z) = -\frac{1}{2}\frac{1}{\pi}\left(\left(-\frac{A_1\phi_1 e^{-\frac{\phi_1 y}{h}}}{h} - \frac{A_2\phi_2 e^{-\frac{\phi_2 y}{h}}}{h} - \frac{(-1-A_1-A_2)\phi_3 e^{-\frac{\phi_3 y}{h}}}{h}\right) h\sum_{m=1}^{n}\frac{C_m}{m}\sin\left(\frac{2m\pi z}{h}\right)\right)$$

$$\tau_{yz}(y,z) = -\frac{1}{2}\frac{\left(-\frac{\phi_2\phi_1 e^{-\frac{\phi_1 y}{h}}}{(\phi_1-\phi_2)h} - \frac{\phi_2\phi_1 e^{-\frac{\phi_2 y}{h}}}{(\phi_2-\phi_1)h}\right) h\left(\sum_{m=1}^{n}\frac{D_m\sin\left(\frac{2m\pi z}{h}\right)}{m}\right)}{\pi}$$

$$\sigma_z(y,z) = \frac{1}{4}\frac{\phi_2\phi_1\left(e^{-\frac{\phi_1 y}{h}}\phi_1 - e^{-\frac{\phi_2 y}{h}}\phi_2\right)\left(\sum_{m=1}^{n}\frac{D_m\left(-\cos\left(\frac{2m\pi z}{h}\right)+\cos(m\pi)\right)}{m^2}\right)}{(\phi_1-\phi_2)\pi^2}$$

Table 4: Stress functions after BCs and equilibrium

There are some matters that remain to be discussed concerning the functions as they are presented in the table above.

First of all, the f(y) function that appears in the function of σ_z was placed in order to satisfy the top and bottom ply condition for the mentioned stress, also accounting for the fact (from the form of f(y) finally) that σ_z should be zero when the far-field is reached and y goes to infinity.

The Fourier coefficients, namely C_m and D_m that appear in the functions will be found by matching the limit of the stress expressions as y goes to infinity with the corresponding CLPT solution.

Looking at Table 4 with the stresses, one can see that actually when y approaches the far-field (y large), the out-of-plane stresses become zero, while the in-plane ones have a remaining part, consisting of the Fourier series multiplied by some coefficients. In each case, these parts are set equal to the corresponding stress solution provided by CLPT for each ply.

Specifically for the case of σ_x, an extra coefficient K is required, because a Fourier cosine series averages to zero but, unlike σ_y and τ_{xy}, whose CLPT solution averages to zero through the thickness, σ_x does not. The way all the coefficients are calculated is described in detail later, in section (3.4.3.1).

3.4 Energy Expression Minimization

After determining all the stress expressions, the energy of the laminate can be found.

3.4.1 Formulation of the energy expression

In order to calculate the total energy of the laminate, some matrices need to be defined first. The required ones are the compliance matrix, as well as the three-dimensional stress tensor. These are defined using the three-dimensional stress-strain relation, solved with respect to strains:

$$\begin{bmatrix} \varepsilon_x \\ \varepsilon_y \\ \varepsilon_z \\ \gamma_{yz} \\ \gamma_{xz} \\ \gamma_{xy} \end{bmatrix} = \begin{bmatrix} S_{11} & S_{12} & S_{13} & 0 & 0 & S_{16} \\ S_{12} & S_{22} & S_{23} & 0 & 0 & S_{26} \\ S_{13} & S_{23} & S_{33} & 0 & 0 & S_{36} \\ 0 & 0 & 0 & S_{44} & S_{45} & 0 \\ 0 & 0 & 0 & S_{45} & S_{55} & 0 \\ S_{16} & S_{26} & S_{36} & 0 & 0 & S_{66} \end{bmatrix} \cdot \begin{bmatrix} \sigma_{xx} \\ \sigma_{yy} \\ \sigma_{zz} \\ \tau_{yz} \\ \tau_{xz} \\ \tau_{xy} \end{bmatrix} \tag{23}$$

From which the compliance tensor is obtained as:

$$[C] = \begin{bmatrix} S_{11} & S_{12} & S_{13} & 0 & 0 & S_{16} \\ S_{12} & S_{22} & S_{23} & 0 & 0 & S_{26} \\ S_{13} & S_{23} & S_{33} & 0 & 0 & S_{36} \\ 0 & 0 & 0 & S_{44} & S_{45} & 0 \\ 0 & 0 & 0 & S_{45} & S_{55} & 0 \\ S_{16} & S_{26} & S_{36} & 0 & 0 & S_{66} \end{bmatrix} \tag{24}$$

It must be noted at this point that the elements of the compliance matrix are on a ply basis. The respective calculations will be given below at the end of section 3.4.4. The expression for the complementary energy of the laminate is given as:

$$U = \int_0^{infinity} \int_{-\frac{h}{2}}^{\frac{h}{2}} \frac{1}{2} \cdot [A]^T \cdot [C] \cdot [A] \, dz \, dy \tag{25}$$

In the formula above, [A] is the stress vector as given below:

$$[A] = \begin{bmatrix} \sigma_x \\ \sigma_y \\ \sigma_z \\ \tau_{yz} \\ \tau_{xz} \\ \tau_{xy} \end{bmatrix} \tag{26}$$

The superscript "T" indicates the transpose of matrix [A]. Normally, the above formula should include a triple integration over the volume. Taking into account that no dependence on x is considered, the energy expression diminishes to the above.
By performing the matrix operations of the above equation, we get to the following form of the energy expression:

$$U = \iint \Big(\frac{1}{2} S_{11} \sigma_x^2 + \sigma_x S_{12} \sigma_y + \sigma_x S_{13} \sigma_z + \sigma_x S_{16} \tau_{xy} + \frac{1}{2} S_{22} \sigma_y^2 + \sigma_y S_{23} \sigma_z + \sigma_y S_{26} \tau_{xy} + \frac{1}{2} S_{33} \sigma_z^2 + \sigma_z S_{36} \tau_{xy} + \frac{1}{2} S_{44} \tau_{yz}^2 + \tau_{yz} S_{45} \tau_{xz} + \frac{1}{2} S_{55} \tau_{xz}^2 + \frac{1}{2} S_{66} \tau_{xy}^2 \Big) \, dy \, dz \tag{27}$$

This equation consists of 13 terms in total. The next step is integrations with respect to y and z. It should be emphasized at this point that for each one of the stress expressions (and correspondingly the same holds for each one of the energy terms), the dependence on y is separated from the dependence on z.
This means that each one of the energy terms will be firstly integrated with respect to y and then at a second step with respect to z.
Moreover, by taking a look at the given compliance matrix, one would assume that some of the matrix elements will be zero, since the approach concerns at this point only symmetric laminates. This is actually true, namely for S_{16}, S_{26}, S_{36} and S_{45}. But this is true if someone considers the compliances of the whole laminate. For the scope of the present analysis and in order to evaluate the energy accurately, the compliances are considered as ply compliances. In this way, each ply will have its own contribution, multiplied by a different factor.
Therefore, for the coming sections, whenever compliance is stated, it will be on a ply basis. In other words, S_{ij} is considered to be a z dependent parameter. Hence, it will be included in the z integration.

3.4.2 Integration with respect to y

The dependence of the stress functions on y is in terms of the exponential part of the functions. The integration limits in this case are zero and infinity. Zero indicates the free edge of the plate and infinity the part of the laminate towards the center, at which the interlaminar stresses become zero. As a reference, the procedure will be shown for the first term of the energy expression. The rest of the terms are treated in the same manner and the calculations can be seen in the appendix.

Before going into the calculations, it must be mentioned that for ease of manipulation of the terms, the Fourier parts of each function, together with the compliance terms that are also depending on z are replaced by S_1..S_7. Each one of these terms is given for clarification.

stress	Corresponding S_k term (k=1…7)
σ_x	$S_1 = \frac{S_{12}\left(\sum_{m=1}^{n} D_m \cos\left(\frac{2m\pi z}{h}\right)\right)}{S_{11}} \qquad S_2 = \frac{S_{13}\left(\sum_{m=1}^{n} \frac{D_m \cos\left(\frac{2m\pi z}{h}\right)}{m^2}\right)}{S_{11}}$
σ_y	$S_3 = \sum_{m=1}^{n} D_m \cos\left(\frac{2m\pi z}{h}\right)$
σ_z	$S_4 = \sum_{m=1}^{n} \frac{D_m\left(\cos(m\pi) - \cos\left(\frac{2m\pi z}{h}\right)\right)}{m^2}$
τ_{xz}	$S_5 = \sum_{m=1}^{n} \frac{C_m \sin\left(\frac{2m\pi z}{h}\right)}{m}$
τ_{yz}	$S_6 = \sum_{m=1}^{n} \frac{D_m \sin\left(\frac{2m\pi z}{h}\right)}{m}$
τ_{xy}	$S_7 = \sum_{m=1}^{n} C_m \cos\left(\frac{2m\pi z}{h}\right)$

Table 5: z dependent parts of stress functions

Continuing, now that the z parts of the functions have been replaced by the S_k terms, they can be considered solely as functions of y for that step. As it can be seen from the energy expression, the first term is $(\sigma_x)^2$. Therefore, the required integration is:

$$\int_0^{\infty} \sigma_x(y)^2 \, dy \quad (28)$$

For some of the terms of the energy expression, the whole integral goes to infinity and this is caused by parts that are directly multiplied by infinity in the upper bound of the integration. Hence, whenever an issue like that occurs, infinity is replaced by a new unknown denoted L that can be viewed as the "boundary layer" within which interlaminar stresses are appreciable. It is a sufficiently large number that will be determined later on. Furthermore, for the simplification of the integrated terms, the values of φ_1, φ_2 and φ_3 are always considered to be positive. Carrying out the calculations, the final form of the first term of the energy expression after y integration is:

$$\begin{aligned} term1 = {} & \frac{1}{32} \frac{\left(32 L \pi^4 \phi_1^2 \phi_2 + 32 L \pi^4 \phi_1 \phi_2^2 - 48 \pi^4 h \phi_1^2 - 80 \pi^4 h \phi_1 \phi_2 - 48 \pi^4 h \phi_2^2\right) S_1^2}{\phi_1 \phi_2 \left(\phi_1 + \phi_2\right) \pi^4} + \Bigg(\\ & -\frac{1}{4} \frac{h \phi_1 \phi_2 S_2}{\pi^2 \left(\phi_1 + \phi_2\right)} + \frac{1}{32} \frac{1}{\phi_1 \phi_2 \left(\phi_1 + \phi_2\right) \pi^4} \Big(-32 L \pi^4 K_{star} \phi_1^2 \phi_2 \\ & - 32 L \pi^4 K_{star} \phi_1 \phi_2^2 + 64 \pi^4 h K_{star} \phi_1^2 + 128 \pi^4 h K_{star} \phi_1 \phi_2 + 64 \pi^4 h K_{star} \phi_2^2 \Big) \Bigg) S_1 \\ & + \frac{1}{32} \frac{h \phi_1^2 \phi_2^2 S_2^2}{\left(\phi_1 + \phi_2\right) \pi^4} + \frac{1}{32} \frac{32 L \pi^4 K_{star}^2 \phi_1^2 \phi_2 + 32 L \pi^4 K_{star}^2 \phi_1 \phi_2^2}{\phi_1 \phi_2 \left(\phi_1 + \phi_2\right) \pi^4} \end{aligned}$$

The exact same procedure holds for the rest of the 13 terms in total. This results in 13 expressions in the form of the one given above for term1. The next step is to perform the z integration.

3.4.3 Integration with respect to z

After integrating the 13 terms with respect to y exactly as shown for the first term, the resulting equations are replaced in the initial energy expression, shown in section 3.4.1. This leads to an expression consisting of the unknown constants φ_1, φ_2, φ_3, A_1 and A_2, h which is the total laminate thickness and the z dependent parameters S_k, the compliance elements S_{ij}, the Fourier series and K_{star}.

Again, in order to make calculations easier and more straightforward, all the parts that have a z dependence are grouped together and substituted by the corresponding T_j terms. These terms that are 22 in total and include different combinations of S_{ij}, S_k, K_{star}. They are given in the table below.

$T_1 = S_{11} \cdot S_1^2$	$T_{12} = S_{23} \cdot S_3 \cdot S_4$
$T_2 = S_{11} \cdot S_1 \cdot S_2$	$T_{13} = S_{33} \cdot S_4^2$
$T_3 = S_{11} \cdot K_{star} \cdot S_1$	$T_{14} = S_{44} \cdot S_6^2$
$T_4 = S_{11} \cdot S_2^2$	$T_{15} = S_{55} \cdot S_5^2$
$T_5 = S_{11} \cdot K_{star}^2$	$T_{16} = S_{66} \cdot S_7^2$
$T_6 = S_{12} \cdot S_1 \cdot S_3$	$T_{17} = S_{16} \cdot S_1 \cdot S_7$
$T_7 = S_{12} \cdot S_2 \cdot S_3$	$T_{18} = S_{16} \cdot K_{star}$
$T_8 = S_{12} \cdot K_{star} \cdot S_3$	$T_{19} = S_2 \cdot S_{16}$
$T_9 = S_{13} \cdot S_1 \cdot S_4$	$T_{20} = S_{26} \cdot S_3 \cdot S_7$
$T_{10} = S_{13} \cdot S_2 \cdot S_4$	$T_{21} = S_{36} \cdot S_4 \cdot S_7$
$T_{11} = S_{22} \cdot S_3^2$	$T_{22} = S_{45} \cdot S_5 \cdot S_6$

Table 6: Final terms for z integration

Again here, as a reference, the z integration of T_1 will be shown. The same procedure holds for the rest of these terms and more information can be found in the appendix.
First of all, all the operations between series were performed according to the following rule:

$$\sum_{m=1}^{n} A_m \cdot \cos\left(\frac{2 \cdot m \cdot \pi \cdot z}{h}\right) \cdot \sum_{p=1}^{n} B_m \cdot \cos\left(\frac{2 \cdot p \cdot \pi \cdot z}{h}\right) =$$
$$\begin{cases} \sum_{m=1}^{n} \sum_{p=1}^{n} A_m \cdot B_p \cdot \cos\left(\frac{2 \cdot m \cdot \pi \cdot z}{h}\right) \cdot \cos\left(\frac{2 \cdot p \cdot \pi \cdot z}{h}\right) & m \neq p \\ \sum_{m=1}^{n} \left(A_m \cdot \cos\left(\frac{2 \cdot m \cdot \pi \cdot z}{h}\right)\right)^2 & m = p \end{cases}$$

In the second case, where m=p, the square of the Fourier series is handled as shown in the formula below:

$$\sum_{m=1}^{n}\left(A_m\cdot\cos\left(\frac{2\cdot m\cdot\pi\cdot z}{h}\right)\right)^2=\sum_{m=1}^{n}A_m\cdot\cos\left(\frac{2\cdot m\cdot\pi\cdot z}{h}\right)\cdot\sum_{m=1}^{n}A_m\cdot\cos\left(\frac{2\cdot m\cdot\pi\cdot z}{h}\right)=\sum_{m=1}^{n}\sum_{p=1}^{n}A_m\cdot A_p\cdot\cos\left(\frac{2\cdot m\cdot\pi\cdot z}{h}\right)\cdot\cos\left(\frac{2\cdot p\cdot\pi\cdot z}{h}\right) \quad (31)$$

As it can be seen from the formula above, the product of two series is a Fourier double series. In the case where a series is squared, the same formula is used by multiplying the series with itself. Moreover, the integrals are calculated only for half of the laminate and then doubled, owing to the stacking sequence symmetry. It follows then that the integration of T_1 is as follows:

$$\int_a^b T_1\,dz=\begin{cases}\dfrac{S_{12}^2 D_m D_p}{S_{11}}\left(\left(\frac{1}{4}\dfrac{h\sin\left(\frac{2(\pi m-p\pi)b}{h}\right)}{\pi m-p\pi}+\frac{1}{4}\dfrac{h\sin\left(\frac{2(\pi m+p\pi)b}{h}\right)}{\pi m+p\pi}\right)-\left(\frac{1}{4}\dfrac{h\sin\left(\frac{2(\pi m-p\pi)a}{h}\right)}{\pi m-p\pi}+\frac{1}{4}\dfrac{h\sin\left(\frac{2(\pi m+p\pi)a}{h}\right)}{\pi m+p\pi}\right)\right) & m\neq p\\ \dfrac{1}{2}\dfrac{S_{12}^2 D_m^2 h}{S_{11}\cdot m\cdot\pi}\left(\left(\frac{1}{2}\cos\left(\frac{2m\pi b}{h}\right)\sin\left(\frac{2m\pi b}{h}\right)+\frac{m\pi b}{h}\right)-\left(\frac{1}{2}\cos\left(\frac{2m\pi a}{h}\right)\sin\left(\frac{2m\pi a}{h}\right)+\frac{m\pi a}{h}\right)\right) & m=p\end{cases}$$

Where a and b are two random integration limits. As it has already been mentioned, the compliance terms are considered to be on a ply by ply basis.

Concerning the integration bounds, this means that each integral will have to be split in a number of integrals equal to the number of plies for one half of the laminate. Hence, the integration bounds for all of these integrals will be the z coordinates of the lower and upper interface of each ply.

After z integration of all the terms, the resulting expressions should be calculated and summed for the first n terms. In this case, both m and p were set to 40.

3.4.4 Calculation of the z-dependent parameters (Fourier series coefficients & compliance matrix)

As it has already been mentioned, at the point where the interlaminar stress effects will be negligible, the CLPT stress solution must be recovered. This, of course, concerns the in-plane stresses, while the out-of-plane will go to zero. As a reminder, the remaining parts of the in-plane stress functions after y goes to infinity are given.

$$\sigma_{xfar} = -\frac{S_{12}}{S_{11}} \cdot \sum_{m=1}^{n} D_m \cdot \cos\left(\frac{2 \cdot m \cdot \pi \cdot z}{h}\right) + K_{star} \qquad (32)$$

$$\sigma_{yfar} = \sum_{m=1}^{n} D_m \cdot \cos\left(\frac{2 \cdot m \cdot \pi \cdot z}{h}\right) \qquad (33)$$

$$\tau_{xyfar} = \sum_{m=1}^{n} C_m \cdot \cos\left(\frac{2 \cdot m \cdot \pi \cdot z}{h}\right) \qquad (34)$$

Therefore, these expressions should be equal to the corresponding stress value given from CLPT for each ply. Knowing the ply stresses for a unit load, it is possible to determine the Fourier coefficients C_m and D_m and also K_{star} using standard Fourier series procedures. The method will be shown initially for σ_y as an example.

$$\sigma_{yfar} = \sum_{m=1}^{n} D_m \cdot \cos\left(\frac{2 \cdot m \cdot \pi \cdot z}{h}\right) = \sigma_{yCLPT}(z)$$

$$\Rightarrow \sum_{m=1}^{n} D_m \cdot \cos\left(\frac{2 \cdot m \cdot \pi \cdot z}{h}\right) \cdot \cos\left(\frac{2 \cdot p \cdot \pi \cdot z}{h}\right) = \sigma_{yCLPT}(z) \cdot \cos\left(\frac{2 \cdot p \cdot \pi \cdot z}{h}\right)$$

$$\Rightarrow \int_0^{\frac{h}{2}} \sum_{m=1}^{n} D_m \cdot \cos\left(\frac{2 \cdot m \cdot \pi \cdot z}{h}\right) \cdot \cos\left(\frac{2 \cdot p \cdot \pi \cdot z}{h}\right) dz = \int_0^{\frac{h}{2}} \sigma_{yCLPT}(z) \cdot \cos\left(\frac{2 \cdot p \cdot \pi \cdot z}{h}\right) dz$$

Considering now only the left hand side (LHS) of the equation, this integral depends on whether m is equal or not to p. The two cases are:

$$\boldsymbol{LHS} = \begin{cases} \frac{1}{2} \frac{D_m h \left(m \sin(m\pi) \cos(p\pi) - n \cos(m\pi) \sin(p\pi)\right)}{\pi \left(m^2 - p^2\right)} & m \neq p \\ \frac{1}{4} \frac{D_m h \left(\cos(m\pi) \sin(m\pi) + m\pi\right)}{m\pi} & m = p \end{cases} = \begin{cases} 0 & m \neq p \\ \frac{D_m \cdot h}{4} & m = p \end{cases}$$

It can be seen that only the case of m=p gives a solution, through which it is possible to find D_m after equating the result with the right hand side of the equation above. The integral on the right hand side should be split to as many integrals as the plies of half the laminate.

In each one of the integrals, the limits will be the lower and upper edge of the respective ply. For better understanding, an example of the calculation for a half-laminate with 4 plies will be shown.

$$\frac{D_m \cdot h}{4} = \frac{h}{2 \cdot m \cdot \pi} \cdot \left(\sigma_{yfar}(1\,st\ ply) \cdot \left[\sin\left(\frac{2\,m\,\pi\,z}{h} \right) \right]_{0}^{\frac{h}{8}} + \sigma_{yfar}(2\,nd\ ply) \cdot \left[\sin\left(\frac{2\,m\,\pi\,z}{h} \right) \right]_{\frac{h}{8}}^{\frac{h}{4}} \right. \tag{35}$$

$$\left. + \sigma_{yfar}(3\,rd\ ply) \cdot \left[\sin\left(\frac{2\,m\,\pi\,z}{h} \right) \right]_{\frac{h}{4}}^{\frac{3 \cdot h}{8}} + \sigma_{yfar}(4\,th\ ply) \cdot \left[\sin\left(\frac{2\,m\,\pi\,z}{h} \right) \right]_{\frac{3 \cdot h}{8}}^{\frac{h}{2}} \right)$$

The left hand side, as given above, is set equal to the right hand side, which is split in 4 integrals, one for each ply of half the laminate.

The case of τ_{xy} is exactly analogous to what was shown above. The same formulas are applicable only if D_m is replaced by C_m and of course the transverse stress values from CLPT are replaced by the corresponding shear stresses.

Having already determined D_m, K_{star} can also be calculated through the same procedure as shown above, applied on σ_x. Moreover, as already stated, the compliance matrix elements are considered to be on a ply level and not of the whole laminate.

With these results, the through the thickness dependence for σ_x, σ_y and τ_{xy} away from the free edge (where y is large) for a laminate of the type $[0_2/\theta_2/-\theta_2]_s$ under static tension in the x direction (see Figures 10, 11) predicted by the present model is compared to the CLPT solution in Figures 12 and 13

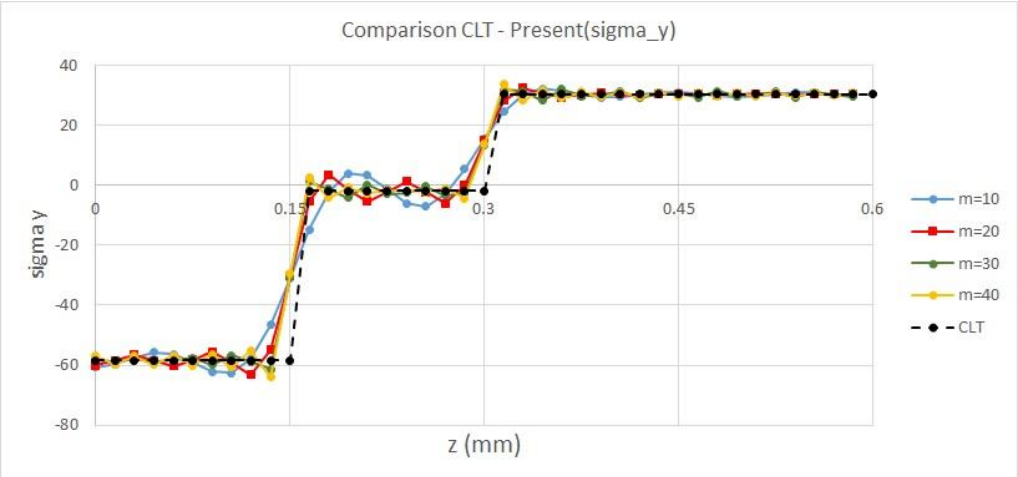

Figure 13: Comparison between CLPT stress solution and Fourier series for different numbers of terms in the series for σy

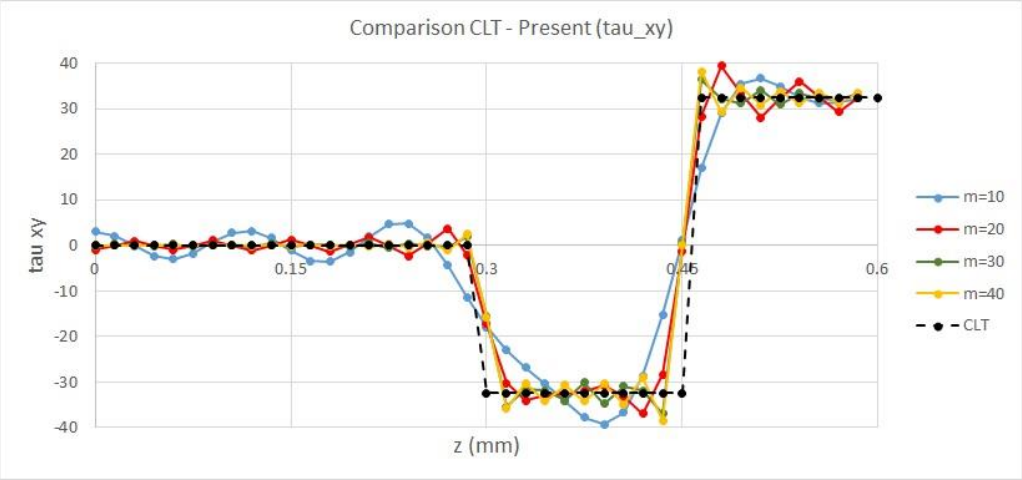

Figure 14: Comparison between CLPT stress solution and Fourier series for different numbers of terms in the series for τxy

It is observed that as the number of terms in the Fourier series increases, the present solution converges to the CLPT solution as it should. Based on the results of Figures 12,13 and similar results for other laminates, it was decided that the number of terms in the Fourier series to be used would be 40. This gives sufficient accuracy and is not very intensive computationally.

The formulas that were used for the determination of the compliances are the following [20]:

$$S_{11} = \left(\frac{1}{E_1}\right)\cdot m^4 + \left(2\cdot\left(-\frac{\nu_{12}}{E_1}\right) + \frac{1}{G_{12}}\right)\cdot m^2\cdot n^2 + \left(\frac{1}{E_2}\right)\cdot n^4$$
$$S_{12} = \left(\frac{1}{E_1} + \frac{1}{E_2} - \frac{1}{G_{12}}\right)\cdot m^2\cdot n^2 + \left(-\frac{\nu_{12}}{E_1}\right)\cdot\left(m^4 + n^4\right)$$
$$S_{13} = \left(-\frac{\nu_{13}}{E_1}\right)\cdot m^2 + \left(-\frac{\nu_{23}}{E_2}\right)\cdot n^2$$
$$S_{22} = \left(\frac{1}{E_1}\right)\cdot n^4 + \left(2\cdot\left(-\frac{\nu_{12}}{E_1}\right) + \frac{1}{G_{12}}\right)\cdot m^2\cdot n^2 + \left(\frac{1}{E_2}\right)\cdot m^4$$
$$S_{23} = \left(-\frac{\nu_{13}}{E_1}\right)\cdot n^2 + \left(-\frac{\nu_{23}}{E_2}\right)\cdot m^2$$
$$S_{33} = \frac{1}{E_3}$$

$$S_{44} = \left(\frac{1}{G_{13}}\right)\cdot n^2 + \left(\frac{1}{G_{23}}\right)\cdot m^2$$
$$S_{55} = \left(\frac{1}{G_{13}}\right)\cdot m^2 + \left(\frac{1}{G_{23}}\right)\cdot n^2$$
$$S_{66} = 4\cdot\left(\frac{1}{E_1} + \frac{1}{E_2} - 2\cdot\left(-\frac{v_{12}}{E_1}\right)\right)\cdot n^2\cdot m^2 + \left(\frac{1}{G_{12}}\right)\cdot\left(n^4 + m^4 - 2\cdot m^2\cdot n^2\right)$$
$$S_{16} = 2\cdot\left(\frac{1}{E_1}\right)\cdot m^3\cdot n - 2\cdot\left(\frac{1}{E_2}\right)\cdot m\cdot n^3 + \left(2\cdot\left(\frac{1}{E_2}\right) + \frac{1}{G_{12}}\right)\cdot\left(m\cdot n^3 - m^3\cdot n\right)$$
$$S_{26} = 2\cdot\left(\frac{1}{E_1}\right)\cdot n^3\cdot m - 2\cdot\left(\frac{1}{E_2}\right)\cdot n\cdot m^3 + \left(2\cdot\left(\frac{1}{E_2}\right) + \frac{1}{G_{12}}\right)\cdot\left(n\cdot m^3 - n^3\cdot m\right)$$
$$S_{36} = 2\cdot\left(\left(-\frac{v_{13}}{E_1}\right) - \left(-\frac{v_{23}}{E_2}\right)\right)\cdot m\cdot n$$
$$S_{45} = \left(\frac{1}{G_{13}} - \frac{1}{G_{23}}\right)\cdot m\cdot n$$

Table 7: Compliance matrix elements calculation

Where m and n represent cos(θ) and sin(θ) respectively, θ being the fiber orientation of each ply.

This m appearing here should not be confused with the "m" in the Fourier series. Also, E_{11}, E_{22}, G_{12}, G_{13}, G_{23} and v_{12} are basic ply engineering constants experimentally determined.

After having calculated the cumulative value of every integral for the specified number of terms to be accounted, the energy expression has reached its final form, being a polynomial function of φ_1, φ_2, φ_3, A_1, A_2 and L.

L is considered to be a constant and its value has originally been set equal to the whole laminate thickness. It is a value that will be corrected later on and be set equal to the distance from the free edge to the point that the interlaminar stresses go to zero, as it will be observed from the stress plots. The other constraint, as already mentioned, is that φ_1, φ_2 and φ_3 must be greater than zero, in order to satisfy the anticipated exponential decay of the stress expressions.

The last step that needs to be taken before proceeding to the minimization of the energy is the calculation of the work term (described in section 3.4.5).

3.4.5 Work term

The work term is an integral of σ_x over the surface where displacements are described of σ_x*u_o and u_o are the constant applied displacements. The stress expression of σ_x must be integrated with respect to y (from zero to infinity) and z (from –h/2 to +h/2). The same procedure as was followed for the rest of the energy terms will also be used here. For additional information, refer to sections 3.4.2 and 3.4.3.

First of all, σ_x is expressed in the following way:

$$\sigma_x := (y) \to -\left(1 + \frac{\phi_2\, e^{-\frac{\phi_1 y}{h}}}{\phi_1 - \phi_2} + \frac{\phi_1\, e^{-\frac{\phi_2 y}{h}}}{\phi_2 - \phi_1}\right)\cdot M_1 + \frac{1}{4}\,\frac{\left(\frac{\phi_2\,\phi_1^2\, e^{-\frac{\phi_1 y}{h}}}{(\phi_1 - \phi_2)\,h^2} + \frac{\phi_1\,\phi_2^2\, e^{-\frac{\phi_2 y}{h}}}{(\phi_2 - \phi_1)\,h^2}\right) h^2 \cdot M_2}{\pi^2} + M_3 \tag{36}$$

Where,

$$M_1 = \frac{S_{12}}{S_{11}}\cdot D_m \cdot \cos\left(\frac{2\cdot m\cdot \pi \cdot z}{h}\right) \tag{37}$$

$$M_2 = \frac{S_{13}}{S_{11}}\cdot \frac{D_m}{m^2}\cdot \cos\left(\frac{2\cdot m\cdot \pi \cdot z}{h}\right) \tag{38}$$

$$M_3 = K_{star} \tag{39}$$

M_1, M_2, M_3 are all the z-dependent parameters of the expression. By carrying out the double integration of the above expression exactly as described previously, the resulting work term is the following:

$$\left(-\frac{L\,M_1\,\phi_1\,\phi_2 - L\,M_3\,\phi_1\,\phi_2 - h\,M_1\,\phi_1 - h\,M_1\,\phi_2}{\phi_2\,\phi_1}\right)\cdot u_o \tag{40}$$

The constant applied displacement that is needed for the calculation of the work term can be correlated to the externally applied load per unit width N_x. The way to do that is shown below:

$$\begin{bmatrix} N_x \\ N_y \\ N_{xy} \end{bmatrix} = \begin{bmatrix} A_{11} & A_{12} & A_{16} \\ A_{12} & A_{22} & A_{26} \\ A_{16} & A_{26} & A_{66} \end{bmatrix} \cdot \begin{bmatrix} \varepsilon_x \\ \varepsilon_y \\ \gamma_{xy} \end{bmatrix} \qquad (41)$$

In our case, N_x is the only applied load. Hence, N_y and N_{xy} are zero. By solving the system of the 3 equations given in matrix form above, we get to the following:

$$\varepsilon_y = \left(-\frac{A_{12}}{A_{22}} - \frac{A_{12} \cdot A_{26}^2 - A_{16} \cdot A_{22} \cdot A_{26}}{A_{22}^2 \cdot A_{66} - A_{22} \cdot A_{26}^2} \right) \cdot \varepsilon_x \qquad (42)$$

$$\gamma_{xy} = \left(\frac{A_{12} \cdot A_{26} - A_{16} \cdot A_{22}}{A_{22} \cdot A_{66} - A_{26}^2} \right) \cdot \varepsilon_x \qquad (43)$$

Through which it is possible to express ε_x with respect to the applied N_x, if the above are substituted in the first equation of the system, namely:

$$N_x = A_{11} \cdot \varepsilon_x + A_{12} \cdot \varepsilon_y + A_{16} \cdot \gamma_{xy} \qquad (44)$$

Finally, ε_x is the displacement u_o, divided by the length of the laminate l. in this way, the applied displacement can be expressed with respect to the applied load, as shown below:

$$u_o = \frac{N_x \cdot \left(A_{22} A_{66} - A_{26}^2 \right) l}{A_{11} A_{22} A_{66} - A_{11} A_{26}^2 - A_{12}^2 A_{66} + 2 A_{12} A_{16} A_{26} - A_{16}^2 A_{22}} \qquad (45)$$

Where l is the laminate length. With the work term calculated, it is time to start with the minimization of the laminate's energy. The next section discusses that matter.

3.4.6 Energy minimization process

Having performed all the above steps, the next objective is to find the solution that satisfies the requirements stated previously and minimizes the energy expression. The minimization process in that case was approached with two different methods.

In the first case, from the energy expression's final form, the partial derivatives with respect to each one of the 5 variables (φ_1, φ_2, φ_3, A_1, A_2) individually were found.

These derivatives were then treated as a 5x5 system of equations. The algorithm consisted of nested iterations.

Each time, arbitrary values close to anticipated ones were set to three of the five variables and a convergence procedure followed between the two remaining ones.

Once convergence was reached, these two recalculated the value of the third variable (with the preset value) and then a new iteration began. At some point, convergence was satisfied for all five variables.

Another (not so practical) idea that was tried was to actually find all the solutions of the 5x5 system and firstly keep only those ones that satisfy the constraints. At a second step, for all the solutions that were kept, the energy expression value would be calculated and then the set of solutions that gave the minimum value in the energy would be the selected one. Unfortunately, the first step of calculating all the possible solutions of the system turned out to be much more consuming in computational time and power than was expected.

The alternative approach was to minimize the value of the energy expression directly, without using the derivatives.

The inherent limitation of that method is that, even in the case that a minimum is found, it cannot be reassured that this is the global minimum. In fact, it will most likely be a local minimum.

This problem was treated with Matlab's "fconmin" function, as well as Microsoft Excel's optimizer. The issue mentioned above for those tools is due to the built-in algorithms of these optimization functions. When the optimizer enters a valley-like region in space, from that point onwards it will only search vertically for better solutions, thus reaching at some point the bottom of the valley and claiming convergence. Once that happens, the process will end, without checking whether there is another valley in a specific vicinity that goes even lower. So, unless someone has to deal with a convex problem that by default has only one global minimum, this method can prove to be a bit problematic.

A partial solution to the problem would be to change the search process to a more robust one that will jump arbitrarily from one region to another in order to minimize the possibility of falling into the same valley endlessly. After stating the above, it should be reminded that the desired solution to the energy minimization task corresponds to a specific laminate. For different stacking sequences the described procedure concerning the energy expression will have to be repeated.

4 Results

4.1 General Comments

After finding the set of values of the unknowns that minimizes the total energy of the laminate, the solution can be implemented in the stress expressions, so that they can be plotted for a specified point through the thickness of the laminate.

As it was mentioned in the previous chapter (see section 3.4.6), the process of minimizing the energy expression can prove to be quite tricky. The level of complexity of solving the system (or finding the solution that minimizes the energy) is of course directly connected to the number of unknown constants.

Due to the aforementioned issues, the initial 5x5 system (owing to φ_1, φ_2, φ_3, A_1, A_2) had to be reduced in order to get to a solution that would lead to capturing the desired behavior. More specifically, the five unknowns are reduced to 3 by eliminating φ_3 and setting A_1 to zero. The procedure steps are exactly the same as shown in Chapter 3.

4.2 Material Properties & Load Case

The material system that was used in the calculations is CFRP, consisting of unidirectional carbon reinforcement and epoxy resin system. The ply properties that are taken into account are given in the table below:

Property	Value
E_1 (GPa)	137.90
E_2 (GPa)	14.48
E_3 (GPa)	14.48
G_{12} (GPa)	5.86
G_{13} (GPa)	5.86
G_{23} (GPa)	5.86
V_{12} (-)	0.21
V_{13} (-)	0.21
V_{23} (-)	0.21
t_{ply} (mm)	0.15

Table 8: Ply properties of the considered material

Furthermore, the stacking sequence that has been used to get to the stress plots that will be shown further on in the chapter is $[45/-45/0/90]_s$. As a reference for now but also for later on, a sketch is given showing the upper half of the laminate.

Figure 15: Upper half of discussed laminate

Finally, the load case that the upcoming graphs correspond to is shown in the sketch below:

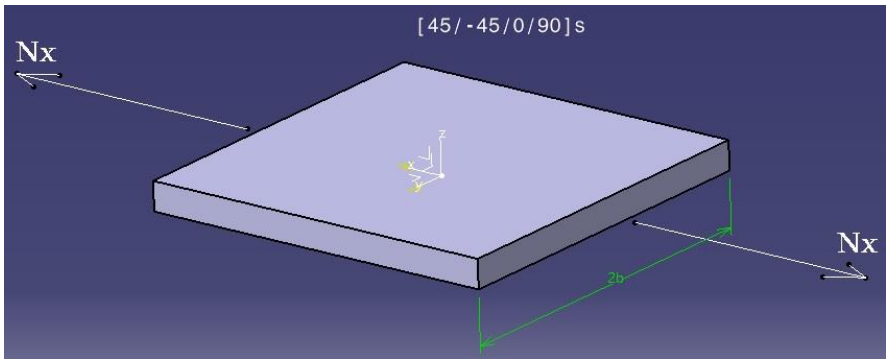

Figure 16: Load case and coordinate system definition

4.3 Simplified Stress Expressions

As it was mentioned in section 4.1, the stress expressions that were introduced and those that were derived from them in Chapter 3 were simplified in order to decrease the required computational time and power. All the steps that lead to the solution of the system are precisely as described in the previous chapters. The simplified stress expressions after satisfying the equilibrium equations and applying the boundary conditions are given below:

$$\sigma_x(y,z)=\left(-\frac{S_{12}}{S_{11}}\right)\left(1+\frac{\phi_2 e^{\frac{-\phi_1 y}{h}}}{\phi_1-\phi_2}-\frac{\phi_1 e^{\frac{-\phi_2 y}{h}}}{\phi_1-\phi_2}\right)\sum_{m=1}^{n} D_m \cos\left(\frac{2m\pi z}{h}\right)$$ $$+\left(\frac{S_{13}}{S_{11}}\right)\left(\frac{1}{4\pi^2}\right)\left(\frac{\phi_1^2\phi_2 e^{\frac{-\phi_1 y}{h}}}{\phi_1-\phi_2}-\frac{\phi_1\phi_2^2 e^{\frac{-\phi_2 y}{h}}}{\phi_1-\phi_2}\right)\sum_{m=1}^{n}\frac{D_m}{m^2}\cos\left(\frac{2m\pi z}{h}\right)+K_{star}$$
$$\sigma_y(y,z)=\left(1+\frac{\phi_2 e^{\frac{-\phi_1 y}{h}}}{\phi_1-\phi_2}-\frac{\phi_1 e^{\frac{-\phi_2 y}{h}}}{\phi_1-\phi_2}\right)\sum_{m=1}^{n} D_m \cos\left(\frac{2m\pi z}{h}\right)$$
$$\sigma_z(y,z)=\left(\frac{-\phi_1\phi_2}{4\pi^2(\phi_1-\phi_2)}\right)\left(\phi_1 e^{\frac{-\phi_1 y}{h}}-\phi_2 e^{\frac{-\phi_2 y}{h}}\right)\sum_{m=1}^{n}\frac{D_m}{m^2}\left(\cos\left(\frac{2m\pi z}{h}\right)-\cos(m\pi)\right)$$
$$\tau_{yz}(y,z)=\left(-\frac{1}{2\pi}\right)\left(\frac{\phi_1\phi_2}{\phi_1-\phi_2}\left(-e^{\frac{-\phi_1 y}{h}}+e^{\frac{-\phi_2 y}{h}}\right)\right)\sum_{m=1}^{n}\frac{D_m}{m}\sin\left(\frac{2m\pi z}{h}\right)$$
$$\tau_{xz}(y,z)=\left(-\frac{1}{2\pi}\right)\phi_2 e^{\frac{-\phi_2 y}{h}}\sum_{m=1}^{n}\frac{C_m}{m}\sin\left(\frac{2m\pi z}{h}\right)$$
$$\tau_{xy}(y,z)=\left(1-e^{\frac{-\phi_2 y}{h}}\right)\sum_{m=1}^{n} C_m \cos\left(\frac{2m\pi z}{h}\right)$$

Table 9: simplified stress plots

4.4 Stress Plots

Using the stress expressions given in Table 9, one can create the corresponding stress plots. In this case, all stresses were plotted along the y axis, moving from the free edge of the laminate towards the center. For the coordinate system that was set refer to Figure 11. In the following sections, the resulting plots will be given, together with some comments on the observed stress behavior.

4.4.1 Out-of-plane stress plots

Concerning the out-of-plane stresses (σ_z, τ_{xz} and τ_{yz}), it is expected by the physics of the phenomenon and correspondingly by the construction of the model that at some point

sufficiently far away from the free edge they will decrease and go asymptotically to zero, thus showing an exponential decay kind of behavior. The respective graphs are given below:

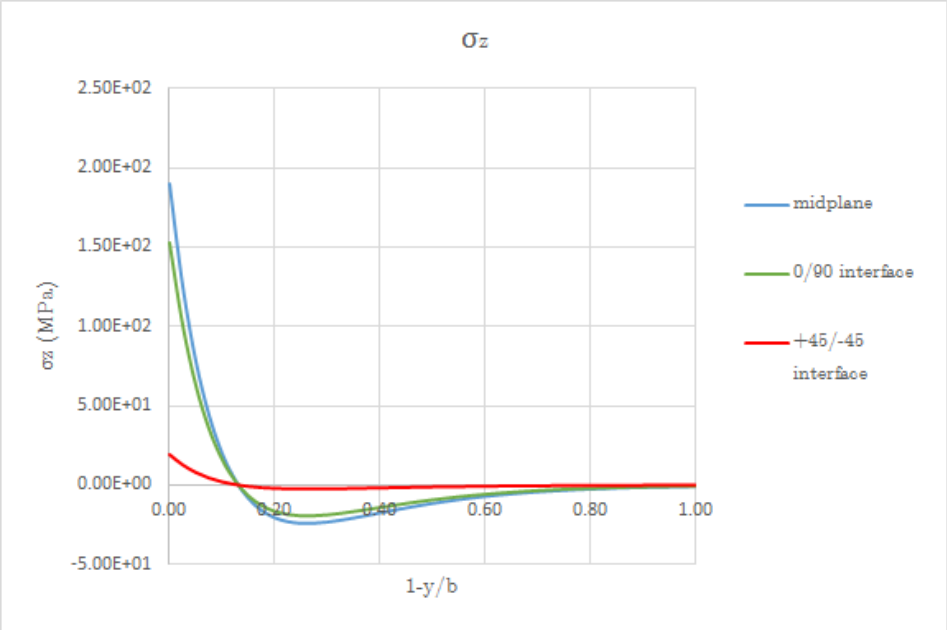

Figure 17: σz along the y-axis in the given coordinates through the thickness

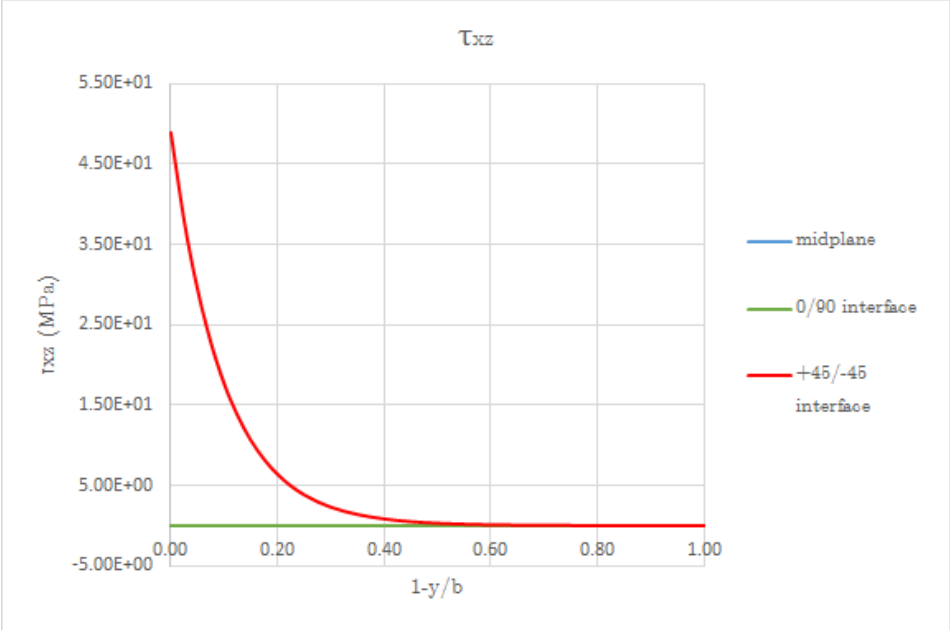

Figure 18: τxz along the y-axis in the given coordinates through the thickness

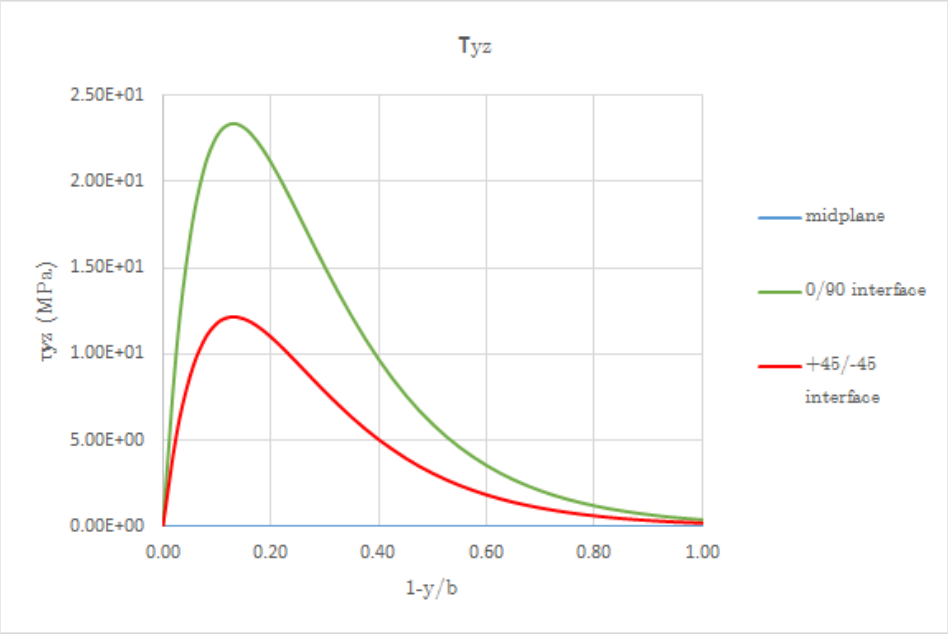

Figure 19: τyz along the y-axis in the given coordinates through the thickness

First of all, it can be seen in Figures 16, 17 and 18 that each one of the stresses has been plotted for three different points along the thickness of the laminate. Namely, at the midplane of the laminate and at the two interfaces along the stacking sequence where there is the largest relative change in fiber orientation between the neighbouring plies. Concerning the horizontal axis, as it has already been mentioned, y initiates at the free edge of the laminate and heads towards the origin of the coordinate system at the center of the laminate (see Figure 11). Moreover, the constant b in (1-y/b) is equal to two times the thickness of the laminate ($=2*n_{plies}*t_{ply}$) [26], [27].

Looking at all three graphs, at h/2 all the out-of-plane stresses are zero (red label in plots). This fact confirms the boundary condition that all the z-acting stresses (σ_z, τ_{xz} and τ_{yz}) are zero at the top and bottom surface of the laminate (see section 3.3.2).

Continuing, all the out-of-plane stresses have the desired exponential decay behaviour and hey go to zero after a specific distance from the free edge. In the model, this "threshold" is considered as infinity in order for the corresponding expressions to become zero. Furthermore, there is a gradual decrease in the values of the ply stresses as one goes towards the upper surface of the laminate, which is also anticipated.

4.4.2 In-plane stress plots

As it was mentioned in the previous section, at some distance from the free edge, the interlaminar stresses will become zero. At this point, the in-plane stresses should recover the CLPT stress solution and remain constant once they reach the corresponding value. This is observed in the graphs given below.

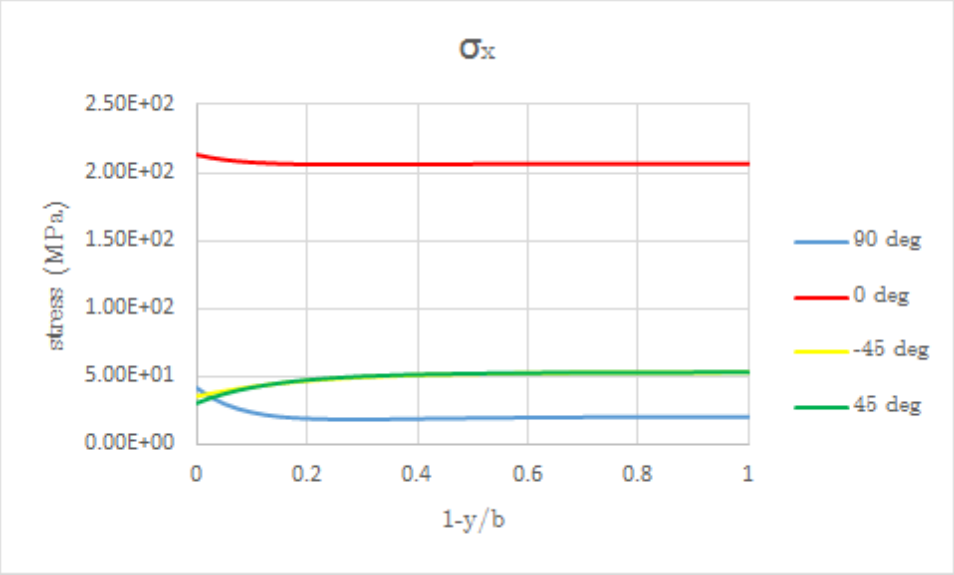

Figure 20: σx along y-axis

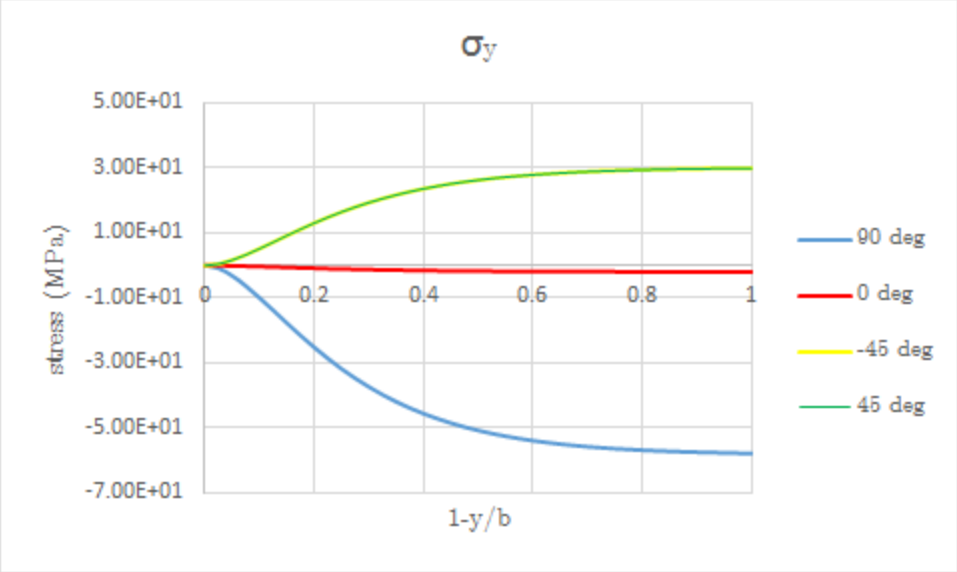

Figure 21: σy along y-axis

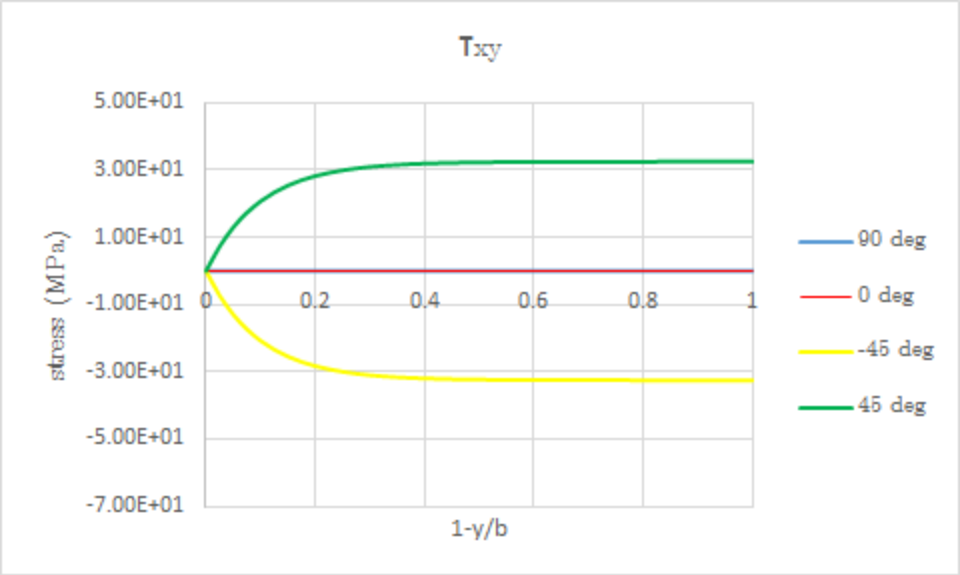

Figure 22: τxy along y-axis

Indeed, the stress values that are obtained from the graph once they become constant match to within less than 0.6% the ones calculated through CLPT, shown below:

	90°	0°	-45°	45°
σ_x (MPa)	20.45	206.62	53.13	53.13
σ_y (MPa)	-58.38	-2.03	30.20	30.20
τ_{xy} (MPa)	0	0	-32.45	32.45

Table 10: CLPT stress values for the given laminate

4.5 Comparison to Literature - Considerations

The out-of-plane stress plots presented above (refer to Figures 17-19) were afterwards compared to the stress results presented in [25]. The comparison showed that, although qualitatively the interlaminar stresses are correct and follow the anticipated trends, the numerical values of the stresses in the two cases differ significantly.

The first question that rises is whether the solution (φ_1, φ_2) of the energy expression minimization is not correct, thus creating the numerical deviation between the model and the literature. In order to check for that, σ_z was plotted again along the transverse distance from the free edge, for all the ply interfaces. This graph is presented below:

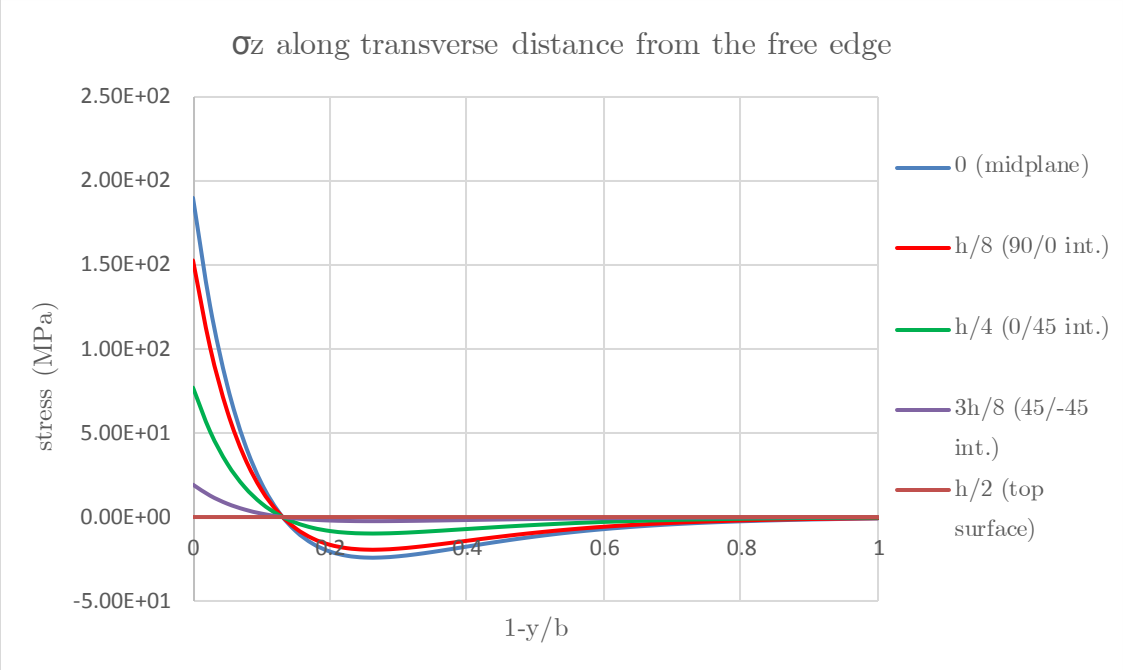

Figure 23: σz along y axis for different z locations

As it can be seen in the graph above, σz becomes zero at the same transverse distance from the free edge (along y-axis), irrespective of the location along the thickness of the laminate. This suggests that there are no anomalous variations on the σz plots that would manifest themselves as wide variations in the location that the stress becomes zero. Solutions that have been published support this fact [25].

After consecutive trials and errors, it was realized that the results are distorted by a multiplicative factor. This factor is carried on from some point and in the end all the stress values are multiplied by that same factor. This factor has been found to be constant for each stress (but each stress having its own unique factor) but it is not known for sure whether it also changes for each one of the plies.

After finding this factor for a certain stress and applying it to the results of the model, the agreement between the present solution and the one presented in [25] is excellent, as it is shown in the figure below:

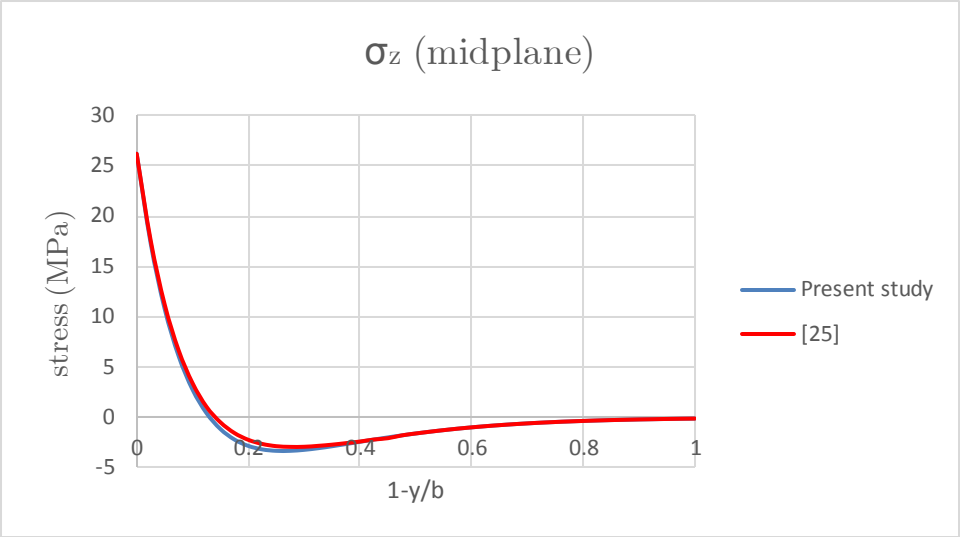

Figure 24: Present results compared to literature after applying the correction factor

With these findings it can be reassured that a multiplicative factor is causing the error and that there is no issue with the approach or the solution of the energy minimization. A respectable amount of time was dedicated to breaking down the code and rewriting multiple scripts in order to check for potential bugs and errors. Furthermore, the whole process for the determination of the final stress expressions and their subsequent implementation in the code was checked from top to bottom thoroughly. Unfortunately, the multiplicative factor was still not found after 2-3 months of checking and at that point there was no more time available, although the specific research topic was highly motivating and intriguing.

Therefore, the model itself in its approach and the symbolic stress expressions are correct and once this factor is found, it can be applied in order to predict the first matrix cracks and subsequently the first local delamination in the discussed class of laminates under tension.

5 Discussion – Recommendations for Future Research

Despite the unexpected issues that occurred in the formulation of the model and were discussed in Section 4.5, the derived expressions are in essence capable of capturing the stress interactions that take place at the vicinity of the free edges of a composite laminate. Each one of the stress expressions has the behaviour that it is expected to have in space and the applied boundary conditions are indeed verified by the stress plots.

Once the factor that distorts the stress values is found, the stress expressions can be implemented in a failure theory such as the Puck criterion that, as discussed in Section 2.5, is capable of accounting for the anticipated damage phenomena. In that way, it will be possible to predict the failure sequence that was presented in [6], [13].

Although at this point it is not causing any errors, the process of the energy minimization could be made more efficient by writing a code that will start with initial values and converge to a solution of the system of equations that minimize the energy of the laminate. Once a solution is found, then the algorithm should jump to a region sufficiently far away from there. This step is suggested in order to ensure that the optimizer will exit the "valley" of the previously found solution. After a sufficient number of iterations, the solution will begin to converge. Once convergence has reached the desirable level, the solution is kept and implemented in the expressions.

Further on, once the model is finalized and it can accurately duplicate the results presented in the aforementioned literature, an interesting continuation of the project would be to implement the developed method in the model of Kassapoglou [28] for the fatigue life evaluation of composite structures, which is based on the cycle-by-cycle probability of failure.

The potential capabilities of such an extension are remarkable, since the field of fatigue of composite structures is in need of a method that does not limit itself in curve fitting in order to capture damage occurrences through conditions and criteria originally designed to describe the behaviour of isotropic materials.

Finally, the model was originally designed to account for either symmetric or non-symmetric laminates, as well as all possible combinations of applied in-plane loads per unit width.

6 References

[1] V. Las, R. Zemcík, T. Kroupa, and R. Kottner, "Failure prediction of composite materials," *Bull. Appl. Mech.*, vol. 4, no. 14, pp. 81–87, 2008.

[2] Z. Hashin, "Analysis of cracked laminates: a variational approach," *Mech. Mater.*, vol. 4, no. 2, pp. 121–136, 1985.

[3] G. Lutz, "The Puck theory of failure in laminates in the context of the new guideline VDI 2014 Part 3," pp. 1–12, 2014.

[4] A. Puck and H. Schürmann, "Failure analysis of FRP laminates by means of physically based phenomenological models," *Compos. Sci. Technol.*, vol. 58, pp. 1045–1067, 1998.

[5] R. Talreja, *Fatigue of Composite Materials*. CRC Press, 1987, pp. 1–196.

[6] T. K. O'Brien, "Characterization of Delamination Onset and Growth in a Composite Laminate," 1981.

[7] M. Caslini, C. Zanotti, and T. K. O'Brien, "Study of Matrix Cracking and Delamination in Glass/Epoxy Laminates," *J. Compos. Technol. Res.*, vol. 9, no. 4, pp. 121–130, 1987.

[8] K. Reifsnider and A. Talug, "Analysis of fatigue damage in composite laminates," *Int. J. Fatigue*, no. January, pp. 3–11, 1980.

[9] G. Dvorak and N. Laws, "Analysis of progressive matrix cracking in composite laminates II. First ply failure," *J. Compos. Mater.*, vol. 21, no. 4, pp. 309–329, Jan. 1987.

[10] J.-F. Berthelot, J. M., Leblond P., Mahi A.EI, Le Corre, "Transverse Cracking of Cross-Ply Laminates:Part1.Analysis," *Compos. Part A*, vol. 27, pp. 989–1001, 1996.

[11] N. Laws, G. Dvorak, and M. Hejazi, "Stiffness changes in unidirectional composites caused by crack systems," *Mech. Mater.*, vol. 2, pp. 123–137, 1983.

[12] J. M. Berthelot, "Analysis of the transverse cracking of cross-ply laminates: a generalized approach," *J. Compos. Mater.*, vol. 31, no. 18, pp. 1780–1805, Sep. 1997.

[13] T. K. O'Brien and S. J. Hooper, "Local Delamination in Laminates with Angle-Ply Matrix Cracks: Part I Tension Tests and Stress Analysis," NASA Langley Research Center, 1991.

[14] C. Kassapoglou, "Fatigue Life Prediction of Composite Structures Under Constant Amplitude Loading," *J. Compos. Mater.*, vol. 41, no. 22, pp. 2737–2754, Nov. 2007.

[15] C. Kassapoglou, "Fatigue Model for Composites Based on the Cycle-by-cycle Probability of Failure: Implications and Applications," *J. Compos. Mater.*, vol. 45, no. 3, pp. 261–277, Oct. 2009.

[16] P. D. Soden, A. S. Kaddour, and M. J. Hinton, "Recommendations for designers and researchers resulting from the world-wide failure exercise," *Compos. Sci. Technol.*, vol. 64, no. 3–4, pp. 589–604, Mar. 2004.

[17] A. Kaddour, M. Hinton, P. Smith, and S. Li, "The background to the third world-wide failure exercise," *J. Compos. Mater.*, vol. 47, no. 20–21, pp. 2417–2426, Sep. 2013.

[18] I. Daniel and O. Ishai, *Engineering mechanics of composite materials*. Oxford University Press, 1994.

[19] C. T. Sun, B. J. Quinn, J. Tao, and D. W. Oplinger, "Comparative Evaluation of Failure Analysis Methods for Composite Laminates," 1996.

[20] C. Kassapoglou, *Design and Analysis of Composite Structures With Applications To Aerospace Structures*. Wiley, 2010, p. 324.

[21] O. Hoffman, "The Brittle Strength of Orthotropic Materials," *J. Compos. Mater.*, vol. 1, no. 2, pp. 200–206, Jan. 1967.

[22] A. Puck and H. Schürmann, "Failure analysis of FRP laminates by means of physically based phenomenological models," *Compos. Sci. Technol.*, vol. 62, no. 12–13 SPECIAL ISSUE, pp. 1633–1662, 2002.

[23] A. Puck, J. Kopp, and M. Knops, "Guidelines for the determination of the parameters in Puck's action plane strength criterion," *Compos. Sci. Technol.*, vol. 62, no. 3, pp. 371–378, 2002.

[24] C. Kassapoglou and P. Lagace, "An efficient method for the calculation of interlaminar stresses in composite materials," *J. ...*, vol. 53, no. December 1986, 1986.

[25] C. Kassapoglou, "Determination of Interlaminar Stresses in Composite Laminates under Combined Loads," *J. Reinf. Plast. Compos.*, vol. 9, no. 1, pp. 33–58, Jan. 1990.

[26] a. S. D. Wang and F. W. Crossman, "Some New Results on Edge Effect in Symmetric Composite Laminates," *J. Compos. Mater.*, vol. 11, no. 1, pp. 92–106, Jan. 1977.

[27] a. S. D. Wang and F. W. Crossman, "Calculation of Edge Stresses in Multi-Layer Laminates by Sub-Structuring," *J. Compos. Mater.*, vol. 12, no. 1, pp. 76–83, Apr. 1978.

[28] C. Kassapoglou and M. Kaminski, "Modeling damage and load redistribution in composites under tension–tension fatigue loading," *Compos. Part A Appl. Sci. Manuf.*, vol. 42, no. 11, pp. 1783–1792, Nov. 2011.

Appendix I – Y Integration of the Energy Expression Terms

First of all, the stresses will be given at their latest form, with all z-dependent parts substituted by S_1 to S_7. For these refer to Table 5 of the report.

$$\sigma_x := (y) \to -\left(1 + \frac{\phi_2 e^{-\frac{\phi_1 y}{h}}}{\phi_1 - \phi_2} + \frac{\phi_1 e^{-\frac{\phi_2 y}{h}}}{\phi_2 - \phi_1}\right) S_1 + \frac{1}{4}\frac{\left(\frac{\phi_2 \phi_1^2 e^{-\frac{\phi_1 y}{h}}}{(\phi_1 - \phi_2) h^2} + \frac{\phi_1 \phi_2^2 e^{-\frac{\phi_2 y}{h}}}{(\phi_2 - \phi_1) h^2}\right) h^2 S_2}{\pi^2} + K_{star} \quad (1)$$

$$\sigma_y := (y) \to \left(1 + \frac{\phi_2 e^{-\frac{\phi_1 y}{h}}}{\phi_1 - \phi_2} + \frac{\phi_1 e^{-\frac{\phi_2 y}{h}}}{\phi_2 - \phi_1}\right) S_3 \quad (2)$$

$$\sigma_z := (y) \to \frac{1}{4}\frac{\phi_1 \phi_2 \left(e^{-\frac{\phi_1 y}{h}} \phi_1 - e^{-\frac{\phi_2 y}{h}} \phi_2\right) \cdot S_4}{(\phi_1 - \phi_2) \pi^2} \quad (3)$$

$$\tau_{xz} := (y) \to -\frac{1}{2}\frac{\left(-\frac{A_1 \phi_1 e^{-\frac{\phi_1 y}{h}}}{h} - \frac{(-1 - A_1) \phi_2 e^{-\frac{\phi_2 y}{h}}}{h}\right) h \cdot S_5}{\pi} \quad (4)$$

$$\tau_{yz} := (y) \to -\frac{1}{2}\frac{\left(-\frac{\phi_2 \phi_1 e^{-\frac{\phi_1 y}{h}}}{(\phi_1 - \phi_2)} - \frac{\phi_1 \phi_2 e^{-\frac{\phi_2 y}{h}}}{(\phi_2 - \phi_1)}\right) S_6}{\pi} \quad (5)$$

$$\tau_{xy} := (y) \to \left(1 + A_1 e^{-\frac{\phi_1 y}{h}} + (-1 - A_1) e^{-\frac{\phi_2 y}{h}}\right) \cdot S_7 \quad (6)$$

The different terms are the following:

$$term1 := (y) \to \left(\sigma_x(y)\right)^2 :$$

$$term2 := (y) \to \sigma_x(y) \cdot \sigma_y(y) :$$

$$term3 := (y) \to \sigma_x(y) \cdot \sigma_z(y) :$$

$$term4 := (y) \to \left(\sigma_y(y)\right)^2 :$$

$$term5 := (y) \to \sigma_y(y)\cdot\sigma_z(y) :$$
$$term6 := (y) \to \left(\sigma_z(y)\right)^2 :$$
$$term7 := (y) \to \left(\tau_{yz}(y)\right)^2 :$$
$$term8 := (y) \to \left(\tau_{xz}(y)\right)^2 :$$
$$term9 := (y) \to \left(\tau_{xy}(y)\right)^2 :$$
$$term10 := (y) \to \sigma_x(y)\cdot\tau_{xy}(y) :$$
$$term11 := (y) \to \sigma_y(y)\cdot\tau_{xy}(y) :$$
$$term12 := (y) \to \sigma_z(y)\cdot\tau_{xy}(y) :$$
$$term13 := (y) \to \tau_{xz}(y)\cdot\tau_{yz}(y) :$$

Notice that at this point, all the stresses are considered to be only a function of y. This is just for ease of calculations. All the S_k elements that represent the z-dependence of the expressions are considered as constants for now. The integrals of the terms w.r.t. y are shown below in their final form. A point that needs to be mentioned here as that for some of the terms (namely 1, 2, 4, 9, 10 and 11), the integral goes to infinity due to direct multiplication of some constant with infinity. In order to resolve that issue, in those cases infinity is replaced directly with an unknown constant L. This L represents the distance from the free edge after which the interlaminar stress effects cease to exist or become negligible.

$$term1 := \frac{1}{32}\,\frac{\left(32\,L\,\pi^4\,\phi_1^2\,\phi_2 + 32\,L\,\pi^4\,\phi_1\,\phi_2^2 - 48\,\pi^4\,h\,\phi_1^2 - 80\,\pi^4\,h\,\phi_1\,\phi_2 - 48\,\pi^4\,h\,\phi_2^2\right)S_1^2}{\phi_1\,\phi_2\left(\phi_1+\phi_2\right)\pi^4}$$
$$+\left(\frac{1}{4}\,\frac{h\,\phi_1\,\phi_2\,S_1\cdot S_2}{\pi^2\left(\phi_1+\phi_2\right)}\right.$$
$$+\frac{1}{32}\,\frac{1}{\phi_1\,\phi_2\left(\phi_1+\phi_2\right)\pi^4}\Big(\Big(-32\,L\,\pi^4\,\phi_1^2\,\phi_2 - 32\,L\,\pi^4\,\phi_1\,\phi_2^2 + 64\,\pi^4\,h\,\phi_1^2$$
$$\left.+\,128\,\pi^4\,h\,\phi_1\,\phi_2 + 64\,\pi^4\,h\,\phi_2^2\right)\cdot K_1\Big)\Big) + \frac{1}{32}\,\frac{h\,\phi_1^2\,\phi_2^2\,S_2^2}{\left(\phi_1+\phi_2\right)\pi^4}$$
$$+\frac{1}{32}\,\frac{\left(32\,L\,\pi^4\,\phi_1^2\,\phi_2 + 32\,L\,\pi^4\,\phi_1\,\phi_2^2\right)\cdot K_2}{\phi_1\,\phi_2\left(\phi_1+\phi_2\right)\pi^4}$$

$$term2 := \frac{1}{8}\frac{\left(-8L\pi^2\phi_1^2\phi_2 - 8L\pi^2\phi_1\phi_2^2 + 12\pi^2 h\phi_1^2 + 20\pi^2 h\phi_1\phi_2 + 12\pi^2 h\phi_2^2\right)S_3 S_1}{\pi^2\left(\phi_1+\phi_2\right)\phi_1\phi_2}$$

$$-\frac{1}{8}\frac{h\phi_1\phi_2 S_3 S_2}{\pi^2\left(\phi_1+\phi_2\right)}$$

$$+\frac{1}{8}\frac{\left(8L\pi^2\phi_1^2\phi_2 + 8L\pi^2\phi_1\phi_2^2 - 8\pi^2 h\phi_1^2 - 16\pi^2 h\phi_1\phi_2 - 8\pi^2 h\phi_2^2\right)\mathrm{K}_3}{\pi^2\left(\phi_1+\phi_2\right)\phi_1\phi_2}$$

$$term3 := \frac{1}{32}\frac{\phi_2\phi_1 S_4 h\left(4\pi^2 S_1 + S_2\phi_1\phi_2\right)}{\left(\phi_1+\phi_2\right)\pi^4}$$

$$term4 := \frac{1}{2}\frac{S_3^2\left(2L\phi_1^2\phi_2 + 2L\phi_1\phi_2^2 - 3h\phi_1^2 - 5h\phi_1\phi_2 - 3h\phi_2^2\right)}{\left(\phi_1+\phi_2\right)\phi_1\phi_2}:$$

$$term5 := -\frac{1}{8}\frac{S_3\cdot S_4\phi_1\phi_2 h}{\left(\phi_1+\phi_2\right)\pi^2}$$

$$term6 := \frac{1}{32}\frac{h S_4^2\phi_2^2\phi_1^2}{\left(\phi_1+\phi_2\right)\pi^4}$$

$$term7 := \frac{1}{8}\frac{S_6^2\phi_1\phi_2 h}{\left(\phi_1+\phi_2\right)\pi^2}$$

$$term8 := \frac{1}{8}\frac{h S_5^2\left(A_1^2\phi_1^2 - 2A_1^2\phi_1\phi_2 + A_1^2\phi_2^2 - 2A_1\phi_1\phi_2 + 2A_1\phi_2^2 + \phi_1\phi_2 + \phi_2^2\right)}{\left(\phi_1+\phi_2\right)\pi^2}$$

$$term9 := \frac{1}{8}\frac{h S_5^2\left(A_1^2\phi_1^2 - 2A_1^2\phi_1\phi_2 + A_1^2\phi_2^2 - 2A_1\phi_1\phi_2 + 2A_1\phi_2^2 + \phi_1\phi_2 + \phi_2^2\right)}{\left(\phi_1+\phi_2\right)\pi^2}$$

$$term10 := \frac{1}{8}\frac{1}{\left(\phi_1+\phi_2\right)\pi^2\phi_1\phi_2}\left(S_7\left(-8L\pi^2\phi_1^2\phi_2 - 8L\pi^2\phi_1\phi_2^2 + 4\pi^2 h A_1\phi_1^2 - 4\pi^2 h A_1\right.\right.$$

$$\left.\left.\phi_2^2 + 12\pi^2 h\phi_1^2 + 16\pi^2 h\phi_1\phi_2 + 8\pi^2 h\phi_2^2\right)S_1\right) - \frac{1}{8}\frac{S_7 h\phi_1\phi_2 S_2}{\left(\phi_1+\phi_2\right)\pi^2}$$

$$+\frac{1}{8}\frac{1}{\left(\phi_1+\phi_2\right)\pi^2\phi_1\phi_2}\left(\left(8L\pi^2\phi_1^2\phi_2 + 8L\pi^2\phi_1\phi_2^2 - 8\pi^2 h A_1\phi_1^2 + 8\pi^2 h A_1\phi_2^2\right.\right.$$

$$\left.\left.-8\pi^2 h\phi_1^2 - 8\pi^2 h\phi_1\phi_2\right)\mathrm{K}_4\right)$$

$$term11 := \frac{1}{2}\frac{S_7 S_3\left(2L\phi_1^2\phi_2 + 2L\phi_1\phi_2^2 - hA_1\phi_1^2 + hA_1\phi_2^2 - 3h\phi_1^2 - 4h\phi_1\phi_2 - 2h\phi_2^2\right)}{\left(\phi_1+\phi_2\right)\phi_1\phi_{27}}$$

$$term12 := -\frac{1}{8}\frac{\phi_1\phi_2 S_4 S_7 h}{\left(\phi_1+\phi_2\right)\pi^2}$$

$$term13 := \frac{1}{8}\frac{h S_5 S_6\phi_1\phi_2}{\left(\phi_1+\phi_2\right)\pi^2}$$

Appendix II – Z Integration of the Energy Expression Terms

After doing the integration of the energy expression terms with respect to y, it is time to do the same procedure for z. The final form of the z-dependent parts of the terms can be seen again in Table 6 of the report. The integrals here are shown for arbitrary bounds a and b (lower and upper respectively). For the calculations, the integrals were split in equal sub-integrals as the number of plies of half the laminate. As has already been mentioned, due to symmetry of the laminate, only half is taken into account and then for the calculations every integral is multiplied by 2.

Firstly, the integrals are given for m≠p.

$$\int_a^b (T_1)\,\mathrm{d}z = \frac{S_{12}^2}{S_{11}} \sum_{m=1}^{n}\sum_{p=1}^{n} \mathrm{D}_m \mathrm{D}_p \left(\frac{1}{4} \frac{h \sin\left(\frac{2(\pi m - p\pi) b}{h} \right)}{\pi m - p\pi} + \frac{1}{4} \frac{h \sin\left(\frac{2(\pi m + p\pi) b}{h} \right)}{\pi m + p\pi} \right) - \frac{S_{12}^2}{S_{11}} \sum_{m=1}^{n}\sum_{p=1}^{n} \mathrm{D}_m \mathrm{D}_p \left(\frac{1}{4} \frac{h \sin\left(\frac{2(\pi m - p\pi) a}{h} \right)}{\pi m - p\pi} + \frac{1}{4} \frac{h \sin\left(\frac{2(\pi m + p\pi) a}{h} \right)}{\pi m + p\pi} \right)$$

$$\int_a^b (T_2)\,\mathrm{d}z = \frac{S_{12} S_{13}}{S_{11}} \sum_{m=1}^{n}\sum_{p=1}^{n} \frac{1}{p^2} \left(\mathrm{D}_m \mathrm{D}_p \left(\frac{1}{4} \frac{h \sin\left(\frac{2(\pi m - p\pi) b}{h} \right)}{\pi m - p\pi} + \frac{1}{4} \frac{h \sin\left(\frac{2(\pi m + p\pi) b}{h} \right)}{\pi m + p\pi} \right) \right) - \frac{S_{12} S_{13}}{S_{11}} \sum_{m=1}^{n}\sum_{p=1}^{n} \frac{1}{p^2} \left(\mathrm{D}_m \mathrm{D}_p \left(\frac{1}{4} \frac{h \sin\left(\frac{2(\pi m - p\pi) a}{h} \right)}{\pi m - p\pi} + \frac{1}{4} \frac{h \sin\left(\frac{2(\pi m + p\pi) a}{h} \right)}{\pi m + p\pi} \right) \right);$$

$$\int_a^b \left(T_3\right) \mathrm{d}z = \frac{1}{2} \frac{K_{star} S_{12} \cdot h}{\pi} \cdot \sum_{m=1}^{n} \mathrm{D}_m \frac{\sin\left(\frac{2 m \pi b}{h}\right)}{m} - \frac{1}{2} \frac{K_{star} S_{12} \cdot h}{\pi} \cdot \sum_{m=1}^{n} \mathrm{D}_m \frac{\sin\left(\frac{2 m \pi a}{h}\right)}{m} :$$

$$\int_a^b \left(T_4\right) \mathrm{d}z = \frac{S_{13}^2}{S_{11}} \sum_{m=1}^{n} \sum_{p=1}^{n} \frac{\mathrm{D}_m \mathrm{D}_p \left(\frac{1}{4} \frac{h \sin\left(\frac{2 \left(\pi m - p \pi\right) b}{h}\right)}{\pi m - p \pi} + \frac{1}{4} \frac{h \sin\left(\frac{2 \left(\pi m + p \pi\right) b}{h}\right)}{\pi m + p \pi} \right)}{m^2 \cdot p^2} - \frac{S_{13}^2}{S_{11}} \sum_{m=1}^{n} \sum_{p=1}^{n} \frac{1}{m^2 \cdot p^2} \left(\mathrm{D}_m \mathrm{D}_p \left(\frac{1}{4} \frac{h \sin\left(\frac{2 \left(\pi m - p \pi\right) a}{h}\right)}{\pi m - p \pi} + \frac{1}{4} \frac{h \sin\left(\frac{2 \left(\pi m + p \pi\right) a}{h}\right)}{\pi m + p \pi} \right) \right) :$$

$$\int_a^b \left(T_5\right) \mathrm{d}z = -a K_{star}^2 S_{11} + b K_{star}^2 S_{11} :$$

$$\int_a^b \left(T_9\right) \mathrm{d}z = \frac{S_{12} S_{13}}{S_{11}} \sum_{m=1}^{n} \sum_{p=1}^{n} \frac{1}{p^2} \left(\mathrm{D}_m \mathrm{D}_p \left(\frac{1}{4} \frac{h \sin\left(\frac{2 m \pi b}{h} - p \pi \right)}{m \pi} \right.\right.$$
$$+ \frac{1}{4} \frac{h \sin\left(\frac{2 m \pi b}{h} + p \pi \right)}{m \pi} - \frac{1}{4} \frac{h \sin\left(\frac{2 \left(\pi m - p \pi\right) b}{h} \right)}{\pi m - p \pi}$$
$$\left.\left. - \frac{1}{4} \frac{h \sin\left(\frac{2 \left(\pi m + p \pi\right) b}{h} \right)}{\pi m + p \pi} \right)\right)$$
$$- \frac{S_{12} S_{13}}{S_{11}} \sum_{m=1}^{n} \sum_{p=1}^{n} \frac{1}{p^2} \left(\mathrm{D}_m \mathrm{D}_p \left(\frac{1}{4} \frac{h \sin\left(\frac{2 m \pi a}{h} - p \pi \right)}{m \pi} \right.\right.$$
$$+ \frac{1}{4} \frac{h \sin\left(\frac{2 m \pi a}{h} + p \pi \right)}{m \pi} - \frac{1}{4} \frac{h \sin\left(\frac{2 \left(\pi m - p \pi\right) a}{h} \right)}{\pi m - p \pi}$$
$$\left.\left. - \frac{1}{4} \frac{h \sin\left(\frac{2 \left(\pi m + p \pi\right) a}{h} \right)}{\pi m + p \pi} \right)\right)$$

$$\int_a^b \left(T_{10}\right) \mathrm{d}z = \frac{S_{13}^2}{S_{11}} \sum_{m=1}^{n} \sum_{p=1}^{n} \frac{1}{m^2 \cdot p^2} \left(\mathrm{D}_m \mathrm{D}_p \left(\frac{1}{4} \frac{h \sin\left(\frac{2 m \pi b}{h} - p \pi \right)}{m \pi} \right.\right.$$
$$+ \frac{1}{4} \frac{h \sin\left(\frac{2 m \pi b}{h} + p \pi \right)}{m \pi} - \frac{1}{4} \frac{h \sin\left(\frac{2 \left(\pi m - p \pi\right) b}{h} \right)}{\pi m - p \pi}$$
$$\left.\left. - \frac{1}{4} \frac{h \sin\left(\frac{2 \left(\pi m + p \pi\right) b}{h} \right)}{\pi m + p \pi} \right)\right)$$
$$- \frac{S_{13}^2}{S_{11}} \sum_{m=1}^{n} \sum_{p=1}^{n} \frac{1}{m^2 \cdot p^2} \left(\mathrm{D}_m \mathrm{D}_p \left(\frac{1}{4} \frac{h \sin\left(\frac{2 m \pi a}{h} - p \pi \right)}{m \pi} \right.\right.$$
$$+ \frac{1}{4} \frac{h \sin\left(\frac{2 m \pi a}{h} + p \pi \right)}{m \pi} - \frac{1}{4} \frac{h \sin\left(\frac{2 \left(\pi m - p \pi\right) a}{h} \right)}{\pi m - p \pi}$$
$$\left.\left. - \frac{1}{4} \frac{h \sin\left(\frac{2 \left(\pi m + p \pi\right) a}{h} \right)}{\pi m + p \pi} \right)\right) :$$

$$\int_a^b \left(T_{11}\right) \mathrm{d}z = S_{22} \sum_{m=1}^{n} \sum_{p=1}^{n} \mathrm{D}_m \mathrm{D}_p \left(\frac{1}{4} \frac{h \sin\left(\frac{2\left(\pi m - p\pi\right) b}{h} \right)}{\pi m - p\pi} + \frac{1}{4} \frac{h \sin\left(\frac{2\left(\pi m + p\pi\right) b}{h} \right)}{\pi m + p\pi} \right) - S_{22} \sum_{m=1}^{n} \sum_{p=1}^{n} \mathrm{D}_m \mathrm{D}_p \left(\frac{1}{4} \frac{h \sin\left(\frac{2\left(\pi m - p\pi\right) a}{h} \right)}{\pi m - p\pi} + \frac{1}{4} \frac{h \sin\left(\frac{2\left(\pi m + p\pi\right) a}{h} \right)}{\pi m + p\pi} \right)$$

$$\int_a^b \left(T_{12}\right) \mathrm{d}z = S_{23} \sum_{m=1}^{n} \sum_{p=1}^{n} \frac{1}{p^2} \left(\mathrm{D}_m \mathrm{D}_p \left(\frac{1}{4} \frac{h \sin\left(\frac{2 m \pi b}{h} - p\pi \right)}{m\pi} + \frac{1}{4} \frac{h \sin\left(\frac{2 m \pi b}{h} + p\pi \right)}{m\pi} - \frac{1}{4} \frac{h \sin\left(\frac{2\left(\pi m - p\pi\right) b}{h} \right)}{\pi m - p\pi} - \frac{1}{4} \frac{h \sin\left(\frac{2\left(\pi m + p\pi\right) b}{h} \right)}{\pi m + p\pi} \right) \right) - S_{23} \sum_{m=1}^{n} \sum_{p=1}^{n} \frac{1}{p^2} \left(\mathrm{D}_m \mathrm{D}_p \left(\frac{1}{4} \frac{h \sin\left(\frac{2 m \pi a}{h} - p\pi \right)}{m\pi} + \frac{1}{4} \frac{h \sin\left(\frac{2 m \pi a}{h} + p\pi \right)}{m\pi} - \frac{1}{4} \frac{h \sin\left(\frac{2\left(\pi m - p\pi\right) a}{h} \right)}{\pi m - p\pi} - \frac{1}{4} \frac{h \sin\left(\frac{2\left(\pi m + p\pi\right) a}{h} \right)}{\pi m + p\pi} \right) \right)$$

$$\int_a^b \left(T_{13}\right) \mathrm{d}z = S_{33} \sum_{m=1}^{n} \sum_{p=1}^{n} \frac{1}{p^2 \cdot m^2} \left(\mathrm{D}_m \mathrm{D}_p \left(\frac{1}{2} \cos\left(m\pi - p\pi\right) b + \frac{1}{2} \cos\left(m\pi + p\pi\right) b \right.\right.$$
$$- \frac{1}{4} \frac{h \sin\left(-m\pi + \frac{2p\pi b}{h} \right)}{p\pi} - \frac{1}{4} \frac{h \sin\left(m\pi + \frac{2p\pi b}{h} \right)}{p\pi}$$
$$- \frac{1}{4} \frac{h \sin\left(\frac{2m\pi b}{h} - p\pi \right)}{m\pi} - \frac{1}{4} \frac{h \sin\left(\frac{2m\pi b}{h} + p\pi \right)}{m\pi}$$
$$\left.\left. + \frac{1}{4} \frac{h \sin\left(\frac{2b\pi (m-p)}{h} \right)}{\pi (m-p)} + \frac{1}{4} \frac{h \sin\left(\frac{2b\pi (m+p)}{h} \right)}{\pi (m+p)} \right) \right)$$
$$- S_{33} \sum_{m=1}^{n} \sum_{p=1}^{n} \frac{1}{p^2 \cdot m^2} \left(\mathrm{D}_m \mathrm{D}_p \left(\frac{1}{2} \cos\left(m\pi - p\pi\right) a + \frac{1}{2} \cos\left(m\pi + p\pi\right) a \right.\right.$$
$$- \frac{1}{4} \frac{h \sin\left(-m\pi + \frac{2p\pi a}{h} \right)}{p\pi} - \frac{1}{4} \frac{h \sin\left(m\pi + \frac{2p\pi a}{h} \right)}{p\pi}$$
$$- \frac{1}{4} \frac{h \sin\left(\frac{2m\pi a}{h} - p\pi \right)}{m\pi} - \frac{1}{4} \frac{h \sin\left(\frac{2m\pi a}{h} + p\pi \right)}{m\pi}$$
$$\left.\left. + \frac{1}{4} \frac{h \sin\left(\frac{2a\pi (m-p)}{h} \right)}{\pi (m-p)} + \frac{1}{4} \frac{h \sin\left(\frac{2a\pi (m+p)}{h} \right)}{\pi (m+p)} \right) \right)$$

$$\int_a^b \left(T_{14}\right) \mathrm{d}z$$
$$= S_{44} \sum_{m=1}^{n} \sum_{p=1}^{n} \frac{\mathrm{D}_m \mathrm{D}_p \left(\frac{1}{4} \frac{h \sin\left(\frac{2b\pi (m-p)}{h} \right)}{\pi (m-p)} - \frac{1}{4} \frac{h \sin\left(\frac{2b\pi (m+p)}{h} \right)}{\pi (m+p)} \right)}{m \cdot p}$$
$$- S_{44} \sum_{m=1}^{n} \sum_{p=1}^{n} \frac{\mathrm{D}_m \mathrm{D}_p \left(\frac{1}{4} \frac{h \sin\left(\frac{2a\pi (m-p)}{h} \right)}{\pi (m-p)} - \frac{1}{4} \frac{h \sin\left(\frac{2a\pi (m+p)}{h} \right)}{\pi (m+p)} \right)}{m \cdot p}$$

$$\int_a^b \left(T_{15}\right) \mathrm{d}z$$

$$= S_{55} \sum_{m=1}^{n} \sum_{p=1}^{n} \frac{C_m C_p \left(\frac{1}{4} \frac{h \sin\left(\frac{2\,b\,\pi\,(m-p)}{h} \right)}{\pi\,(m-p)} - \frac{1}{4} \frac{h \sin\left(\frac{2\,b\,\pi\,(m+p)}{h} \right)}{\pi\,(m+p)} \right)}{m \cdot p}$$

$$- S_{55} \sum_{m=1}^{n} \sum_{p=1}^{n} \frac{C_m C_p \left(\frac{1}{4} \frac{h \sin\left(\frac{2\,a\,\pi\,(m-p)}{h} \right)}{\pi\,(m-p)} - \frac{1}{4} \frac{h \sin\left(\frac{2\,a\,\pi\,(m+p)}{h} \right)}{\pi\,(m+p)} \right)}{m \cdot p}$$

$$\int_a^b \left(T_{16}\right) \mathrm{d}z$$

$$= S_{66} \sum_{m=1}^{n} \sum_{p=1}^{n} \frac{C_m C_p \left(\frac{1}{4} \frac{h \sin\left(\frac{2\,\pi\,(m-p)\,b}{h} \right)}{\pi\,(m-p)} + \frac{1}{4} \frac{h \sin\left(\frac{2\,\pi\,(m+p)\,b}{h} \right)}{\pi\,(m+p)} \right)}{m \cdot p}$$

$$- S_{66} \sum_{m=1}^{n} \sum_{p=1}^{n} \frac{C_m C_p \left(\frac{1}{4} \frac{h \sin\left(\frac{2\,\pi\,(m-p)\,a}{h} \right)}{\pi\,(m-p)} + \frac{1}{4} \frac{h \sin\left(\frac{2\,\pi\,(m+p)\,a}{h} \right)}{\pi\,(m+p)} \right)}{m \cdot p}$$

$$\int_a^b \left(T_{17}\right) \mathrm{d}z = \frac{S_{16} S_{12}}{S_{11}} \sum_{m=1}^{n} \sum_{p=1}^{n} \mathrm{D}_m C_p \left(\frac{1}{4} \frac{h \sin\left(\frac{2\,b\,\pi\,(m-p)}{h} \right)}{\pi\,(m-p)} \right.$$

$$\left. + \frac{1}{4} \frac{h \sin\left(\frac{2\,b\,\pi\,(m+p)}{h} \right)}{\pi\,(m+p)} \right) - \frac{S_{16} S_{12}}{S_{11}} \sum_{m=1}^{n} \sum_{p=1}^{n} \mathrm{D}_m C_p \left(\frac{1}{4} \frac{h \sin\left(\frac{2\,a\,\pi\,(m-p)}{h} \right)}{\pi\,(m-p)} \right.$$

$$\left. + \frac{1}{4} \frac{h \sin\left(\frac{2\,a\,\pi\,(m+p)}{h} \right)}{\pi\,(m+p)} \right)$$

$$\int_a^b \left(T_{18}\right) \mathrm{d}z$$

$$= \frac{S_{16} S_{13}}{S_{11}} \sum_{m=1}^{n} \sum_{p=1}^{n} \frac{\mathrm{D}_m C_p \left(\frac{1}{4} \frac{h \sin\left(\frac{2\pi (m-p) b}{h} \right)}{\pi (m-p)} + \frac{1}{4} \frac{h \sin\left(\frac{2\pi (m+p) b}{h} \right)}{\pi (m+p)} \right)}{m^2}$$

$$- \frac{S_{16} S_{13}}{S_{11}} \sum_{m=1}^{n} \sum_{p=1}^{n} \frac{\mathrm{D}_m C_p \left(\frac{1}{4} \frac{h \sin\left(\frac{2\pi (m-p) a}{h} \right)}{\pi (m-p)} + \frac{1}{4} \frac{h \sin\left(\frac{2\pi (m+p) a}{h} \right)}{\pi (m+p)} \right)}{m^2}$$

$$\int_a^b \left(T_{19}\right) \mathrm{d}z = \frac{1}{2} \frac{S_{16} \cdot h \cdot K_{star}}{\pi} \sum_{m=1}^{n} C_m \frac{\sin\left(\frac{2 m \pi b}{h} \right)}{m}$$

$$- \frac{1}{2} \frac{S_{16} \cdot h \cdot K_{star}}{\pi} \sum_{m=1}^{n} C_m \frac{\sin\left(\frac{2 m \pi a}{h} \right)}{m}$$

$$\int_a^b \left(T_{20}\right) \mathrm{d}z = S_{26} \sum_{m=1}^{n} \sum_{p=1}^{n} \mathrm{D}_m C_p \left(\frac{1}{4} \frac{h \sin\left(\frac{2 b \pi (m-p)}{h} \right)}{\pi (m-p)} + \frac{1}{4} \frac{h \sin\left(\frac{2 b \pi (m+p)}{h} \right)}{\pi (m+p)} \right)$$

$$- S_{26} \sum_{m=1}^{n} \sum_{p=1}^{n} \mathrm{D}_m C_p \left(\frac{1}{4} \frac{h \sin\left(\frac{2 a \pi (m-p)}{h} \right)}{\pi (m-p)} + \frac{1}{4} \frac{h \sin\left(\frac{2 a \pi (m+p)}{h} \right)}{\pi (m+p)} \right)$$

$$\int_a^b (T_{21})\,\mathrm{d}z = S_{36}\sum_{m=1}^{n}\sum_{p=1}^{n}\frac{1}{m^2}\left(\mathrm{D}_m C_p\left(\frac{1}{4}\,\frac{h\sin\left(-m\pi+\frac{2p\pi b}{h}\right)}{p\pi}\right.\right.$$
$$+\frac{1}{4}\,\frac{h\sin\left(m\pi+\frac{2p\pi b}{h}\right)}{p\pi}-\frac{1}{4}\,\frac{h\sin\left(\frac{2b\pi(m-p)}{h}\right)}{\pi(m-p)}$$
$$\left.\left.-\frac{1}{4}\,\frac{h\sin\left(\frac{2b\pi(m+p)}{h}\right)}{\pi(m+p)}\right)\right)$$
$$-S_{36}\sum_{m=1}^{n}\sum_{p=1}^{n}\frac{1}{m^2}\left(\mathrm{D}_m C_p\left(\frac{1}{4}\,\frac{h\sin\left(-m\pi+\frac{2p\pi a}{h}\right)}{p\pi}+\frac{1}{4}\,\frac{h\sin\left(m\pi+\frac{2p\pi a}{h}\right)}{p\pi}\right.\right.$$
$$\left.\left.-\frac{1}{4}\,\frac{h\sin\left(\frac{2a\pi(m-p)}{h}\right)}{\pi(m-p)}-\frac{1}{4}\,\frac{h\sin\left(\frac{2a\pi(m+p)}{h}\right)}{\pi(m+p)}\right)\right)$$

$$\int_a^b (T_{22})\,\mathrm{d}z$$
$$=S_{45}\sum_{m=1}^{n}\sum_{p=1}^{n}\frac{C_m\mathrm{D}_p\left(\frac{1}{4}\,\frac{h\sin\left(\frac{2b\pi(m-p)}{h}\right)}{\pi(m-p)}-\frac{1}{4}\,\frac{h\sin\left(\frac{2b\pi(m+p)}{h}\right)}{\pi(m+p)}\right)}{m\cdot p}$$
$$-S_{45}\sum_{m=1}^{n}\sum_{p=1}^{n}\frac{C_m\mathrm{D}_p\left(\frac{1}{4}\,\frac{h\sin\left(\frac{2a\pi(m-p)}{h}\right)}{\pi(m-p)}-\frac{1}{4}\,\frac{h\sin\left(\frac{2a\pi(m+p)}{h}\right)}{\pi(m+p)}\right)}{m\cdot p}$$

The exact same procedure for m=p leads to the following:

$$\int_a^b (T_1)\,\mathrm{d}z=\frac{1}{2}\,\frac{S_{12}^2\cdot h}{S_{11}\cdot\pi}\sum_{m=1}^{n}\frac{\mathrm{D}_m^2\left(\frac{1}{2}\cos\left(\frac{2m\pi b}{h}\right)\sin\left(\frac{2m\pi b}{h}\right)+\frac{m\pi b}{h}\right)}{m}$$
$$-\frac{1}{2}\,\frac{S_{12}^2\cdot h}{S_{11}\cdot\pi}\sum_{m=1}^{n}\frac{\mathrm{D}_m^2\left(\frac{1}{2}\cos\left(\frac{2m\pi a}{h}\right)\sin\left(\frac{2m\pi a}{h}\right)+\frac{m\pi a}{h}\right)}{m}$$

$$\int_a^b \left(T_2\right) \mathrm{d}z = \frac{1}{2} \frac{S_{12} S_{13}}{S_{11} \cdot \pi} \cdot h \cdot \sum_{m=1}^{n} \frac{\mathrm{D}_m^2 \left(\frac{1}{2} \cos\left(\frac{2 m \pi b}{h} \right) \sin\left(\frac{2 m \pi b}{h} \right) + \frac{m \pi b}{h} \right)}{m^3}$$

$$- \frac{1}{2} \frac{S_{12} S_{13}}{S_{11} \cdot \pi} \cdot h \cdot \sum_{m=1}^{n} \frac{\mathrm{D}_m^2 \left(\frac{1}{2} \cos\left(\frac{2 m \pi a}{h} \right) \sin\left(\frac{2 m \pi a}{h} \right) + \frac{m \pi a}{h} \right)}{m^3}$$

$$\int_a^b \left(T_3\right) \mathrm{d}z = \frac{1}{2} \frac{K_{star} S_{12}}{h \cdot \pi} \sum_{m=1}^{n} \mathrm{D}_m \sin\left(\frac{2 m \pi b}{h} \right) - \frac{1}{2} \frac{K_{star} S_{12}}{h \cdot \pi} \sum_{m=1}^{n} \mathrm{D}_m \sin\left(\frac{2 m \pi a}{h} \right)$$

$$\int_a^b \left(T_4\right) \mathrm{d}z = \frac{1}{2} \frac{S_{13}^2 \cdot h}{S_{11} \cdot \pi} \sum_{m=1}^{n} \frac{\mathrm{D}_m^2 \left(\frac{1}{2} \cos\left(\frac{2 m \pi b}{h} \right) \sin\left(\frac{2 m \pi b}{h} \right) + \frac{m \pi b}{h} \right)}{m^5}$$

$$- \frac{1}{2} \frac{S_{13}^2 \cdot h}{S_{11} \cdot \pi} \sum_{m=1}^{n} \frac{\mathrm{D}_m^2 \left(\frac{1}{2} \cos\left(\frac{2 m \pi a}{h} \right) \sin\left(\frac{2 m \pi a}{h} \right) + \frac{m \pi a}{h} \right)}{m^5}$$

$$\int_a^b \left(T_5\right) \mathrm{d}z = -a K_{star}^2 S_{11} + b K_{star}^2 S_{11}$$

$$\int_a^b \left(T_9\right) \mathrm{d}z$$

$$= \frac{1}{2} \frac{S_{12} S_{13} \cdot h}{S_{11} \cdot \pi} \sum_{m=1}^{n} \frac{1}{m^3} \left(\mathrm{D}_m^2 \left(\cos(m \pi) \sin\left(\frac{2 m \pi b}{h} \right) \right. \right.$$

$$\left. \left. - \frac{1}{2} \cos\left(\frac{2 m \pi b}{h} \right) \sin\left(\frac{2 m \pi b}{h} \right) - \frac{m \pi b}{h} \right) \right)$$

$$- \frac{1}{2} \frac{S_{12} S_{13} \cdot h}{S_{11} \cdot \pi} \sum_{m=1}^{n} \frac{1}{m^3} \left(\mathrm{D}_m^2 \left(\cos(m \pi) \sin\left(\frac{2 m \pi a}{h} \right) \right. \right.$$

$$\left. \left. - \frac{1}{2} \cos\left(\frac{2 m \pi a}{h} \right) \sin\left(\frac{2 m \pi a}{h} \right) - \frac{m \pi a}{h} \right) \right)$$

$$\int_a^b \left(T_{10}\right) \mathrm{d}z$$

$$= \frac{1}{2} \frac{S_{13}^2 \cdot h}{S_{11} \cdot \pi} \sum_{m=1}^{n} \frac{1}{m^5} \left(\mathrm{D}_m^2 \left(\cos\left(m\pi\right) \sin\left(\frac{2\,m\pi\,b}{h} \right) \right.\right.$$
$$\left.\left. - \frac{1}{2} \cos\left(\frac{2\,m\pi\,b}{h} \right) \sin\left(\frac{2\,m\pi\,b}{h} \right) - \frac{m\pi\,b}{h} \right) \right)$$
$$- \frac{1}{2} \frac{S_{13}^2 \cdot h}{S_{11} \cdot \pi} \sum_{m=1}^{n} \frac{1}{m^5} \left(\mathrm{D}_m^2 \left(\cos\left(m\pi\right) \sin\left(\frac{2\,m\pi\,b}{h} \right) \right.\right.$$
$$\left.\left. - \frac{1}{2} \cos\left(\frac{2\,m\pi\,b}{h} \right) \sin\left(\frac{2\,m\pi\,b}{h} \right) - \frac{m\pi\,b}{h} \right) \right)$$

$$\int_a^b \left(T_{11}\right) \mathrm{d}z = \frac{1}{2} \frac{S_{22} \cdot h}{\pi} \sum_{m=1}^{n} \frac{\mathrm{D}_m^2 \left(\frac{1}{2} \cos\left(\frac{2\,m\pi\,b}{h} \right) \sin\left(\frac{2\,m\pi\,b}{h} \right) + \frac{m\pi\,b}{h} \right)}{m}$$
$$- \frac{1}{2} \frac{S_{22} \cdot h}{\pi} \sum_{m=1}^{n} \frac{\mathrm{D}_m^2 \left(\frac{1}{2} \cos\left(\frac{2\,m\pi\,a}{h} \right) \sin\left(\frac{2\,m\pi\,a}{h} \right) + \frac{m\pi\,a}{h} \right)}{m}$$

$$\int_a^b \left(T_{12}\right) \mathrm{d}z$$

$$= \frac{1}{2} \frac{S_{23} \cdot h}{\pi} \sum_{m=1}^{n} \frac{1}{m^3} \left(\mathrm{D}_m^2 \left(\cos\left(m\pi\right) \sin\left(\frac{2\,m\pi\,b}{h} \right) \right.\right.$$
$$\left.\left. - \frac{1}{2} \cos\left(\frac{2\,m\pi\,b}{h} \right) \sin\left(\frac{2\,m\pi\,b}{h} \right) - \frac{m\pi\,b}{h} \right) \right)$$
$$- \frac{1}{2} \frac{S_{23} \cdot h}{\pi} \sum_{m=1}^{n} \frac{1}{m^3} \left(\mathrm{D}_m^2 \left(\cos\left(m\pi\right) \sin\left(\frac{2\,m\pi\,a}{h} \right) \right.\right.$$
$$\left.\left. - \frac{1}{2} \cos\left(\frac{2\,m\pi\,a}{h} \right) \sin\left(\frac{2\,m\pi\,a}{h} \right) - \frac{m\pi\,a}{h} \right) \right)$$

$$\int_a^b \left(T_{13}\right) \mathrm{d}z = S_{33} \sum_{m=1}^{n} \frac{\mathrm{D}_m^2 \left(\cos\left(m\pi\right) b - \frac{1}{2} \frac{h \sin\left(\frac{2\,m\pi\,b}{h} \right)}{m\pi} \right)}{m^4}$$
$$- S_{33} \sum_{m=1}^{n} \frac{\mathrm{D}_m^2 \left(\cos\left(m\pi\right) a - \frac{1}{2} \frac{h \sin\left(\frac{2\,m\pi\,a}{h} \right)}{m\pi} \right)}{m^4}$$

$$\int_a^b \left(T_{14}\right) \mathrm{d}z = \frac{1}{2} \frac{S_{44} \cdot h}{\pi} \sum_{m=1}^{n} \frac{\mathrm{D}_m^2 \left(-\frac{1}{2} \cos\left(\frac{2 m \pi b}{h} \right) \sin\left(\frac{2 m \pi b}{h} \right) + \frac{m \pi b}{h} \right)}{m^3}$$

$$- \frac{1}{2} \frac{S_{44} \cdot h}{\pi} \sum_{m=1}^{n} \frac{\mathrm{D}_m^2 \left(-\frac{1}{2} \cos\left(\frac{2 m \pi a}{h} \right) \sin\left(\frac{2 m \pi a}{h} \right) + \frac{m \pi a}{h} \right)}{m^3}$$

$$\int_a^b \left(T_{15}\right) \mathrm{d}z = \frac{1}{2} \frac{S_{55} \cdot h}{\pi} \sum_{m=1}^{n} \frac{C_m^2 \left(-\frac{1}{2} \cos\left(\frac{2 m \pi b}{h} \right) \sin\left(\frac{2 m \pi b}{h} \right) + \frac{m \pi b}{h} \right)}{m^3}$$

$$- \frac{1}{2} \frac{S_{55} \cdot h}{\pi} \sum_{m=1}^{n} \frac{C_m^2 \left(-\frac{1}{2} \cos\left(\frac{2 m \pi a}{h} \right) \sin\left(\frac{2 m \pi a}{h} \right) + \frac{m \pi a}{h} \right)}{m^3}$$

$$\int_a^b \left(T_{16}\right) \mathrm{d}z = \frac{1}{2} \frac{S_{66} \cdot h}{\pi} \sum_{m=1}^{n} \frac{C_m^2 \left(\frac{1}{2} \cos\left(\frac{2 m \pi b}{h} \right) \sin\left(\frac{2 m \pi b}{h} \right) + \frac{m \pi b}{h} \right)}{m}$$

$$- \frac{1}{2} \frac{S_{66} \cdot h}{\pi} \sum_{m=1}^{n} \frac{C_m^2 \left(\frac{1}{2} \cos\left(\frac{2 m \pi a}{h} \right) \sin\left(\frac{2 m \pi a}{h} \right) + \frac{m \pi a}{h} \right)}{m}$$

$$\int_a^b \left(T_{17}\right) \mathrm{d}z = \frac{1}{2} \frac{S_{16} S_{12} \cdot h}{S_{11} \cdot \pi} \sum_{m=1}^{n} \frac{\mathrm{D}_m C_m \left(\frac{1}{2} \cos\left(\frac{2 m \pi b}{h} \right) \sin\left(\frac{2 m \pi b}{h} \right) + \frac{m \pi b}{h} \right)}{m}$$

$$- \frac{1}{2} \frac{S_{16} S_{12} \cdot h}{S_{11} \cdot \pi} \sum_{m=1}^{n} \frac{\mathrm{D}_m C_m \left(\frac{1}{2} \cos\left(\frac{2 m \pi a}{h} \right) \sin\left(\frac{2 m \pi a}{h} \right) + \frac{m \pi a}{h} \right)}{m}$$

$$\int_a^b \left(T_{18}\right) \mathrm{d}z = -a K_{star} S_{16} + b K_{star} S_{16}$$

$$\int_a^b \left(T_{19}\right) \mathrm{d}z = \frac{1}{2} \frac{S_{16} S_{13} \cdot h}{S_{11} \cdot \pi} \sum_{m=1}^{n} \frac{\mathrm{D}_m \sin\left(\frac{2 m \pi b}{h} \right)}{m^3} - \frac{1}{2} \frac{S_{16} S_{13} \cdot h}{S_{11} \cdot \pi} \sum_{m=1}^{n} \frac{\mathrm{D}_m \sin\left(\frac{2 m \pi a}{h} \right)}{m^3}$$

$$\int_a^b \left(T_{20}\right) \mathrm{d}z = \frac{1}{2} \frac{S_{26} \cdot h}{\pi} \sum_{m=1}^{n} \frac{\mathrm{D}_m C_m \left(\frac{1}{2} \cos\left(\frac{2 m \pi b}{h} \right) \sin\left(\frac{2 m \pi b}{h} \right) + \frac{m \pi b}{h} \right)}{m}$$

$$- \frac{1}{2} \frac{S_{26} \cdot h}{\pi} \sum_{m=1}^{n} \frac{\mathrm{D}_m C_m \left(\frac{1}{2} \cos\left(\frac{2 m \pi a}{h} \right) \sin\left(\frac{2 m \pi a}{h} \right) + \frac{m \pi a}{h} \right)}{m}$$

$$\int_a^b \left(T_{21}\right) \mathrm{d}z$$

$$= \frac{1}{2} \frac{S_{36} \cdot h}{\pi} \sum_{m=1}^{n} \frac{1}{m^3} \left(\mathrm{D}_m C_m \left(\cos(m \pi) \sin\left(\frac{2 m \pi b}{h} \right) \right. \right.$$

$$\left. \left. - \frac{1}{2} \cos\left(\frac{2 m \pi b}{h} \right) \sin\left(\frac{2 m \pi b}{h} \right) - \frac{m \pi b}{h} \right) \right)$$

$$- \frac{1}{2} \frac{S_{36} \cdot h}{\pi} \sum_{m=1}^{n} \frac{1}{m^3} \left(\mathrm{D}_m C_m \left(\cos(m \pi) \sin\left(\frac{2 m \pi a}{h} \right) \right. \right.$$

$$\left. \left. - \frac{1}{2} \cos\left(\frac{2 m \pi a}{h} \right) \sin\left(\frac{2 m \pi a}{h} \right) - \frac{m \pi a}{h} \right) \right)$$